therapy [6–9], or intrathecal administration of enzymes [10,11], for treatment of the brain in LSDs. Such treatments were able to overcome the blood–brain barrier to access brain tissue and exhibit considerable efficacy in brain. However, it is difficult to maintain such efficacy for long periods of time. Repetition of these treatments is not practical because intracranial administration is required for them. On the other hand, the usefulness of intravenous administration is limited because of the blood–brain barrier, except in newborn mice which have an immature barrier. It has been reported that intravenous administration of extremely high doses of enzymes [12–14] or of enzymes that remain in the circulation for long periods [15,16] yielded slight passage through the blood–brain barrier, though with increase in the risk of immune response.

Oral administration of small molecules would be a good and convenient method of treatment of the brain for prolonged periods, such as substrate reduction therapy with *N*-butyldeoxynojirimycin or *N*-butyldeoxygalactonojirimycin for glycosphingolipidoses [17–19] or genistein for mucopolysaccharidoses [20], and chemical chaperone therapy for Fabry disease [21] or GM1-gangliosidosis [22]. However, the efficacy of substrate reduction therapies has thus far been quite limited, and chemical chaperone therapies are not applicable for every type of gene mutation.

GM1 gangliosidosis is an LSD and a progressive neurological disease in humans caused by a genetic defect of lysosomal acid β-galactosidase, which hydrolyses the terminal β-galactosidic residue of ganglioside GM1 and other glycoconjugates. The defects in β-galactosidase activity result in accumulation of ganglioside GM1 in various organs, especially the brain, causing progressive neurodegeneration. In our previous study [2], we injected recombinant adenovirus encoding mouse β-galactosidase cDNA intravenously in β-galactosidase-deficient newborn mice, and showed that vector-mediated β-galactosidase-producing brain cells could reduce ganglioside GM1 accumulation. We showed that β-galactosidase enzyme protein could be secreted as well as taken up by the brain cells and function effectively. However, the efficacy obtained was transient. If sufficient amounts of the defective enzyme could be permanently secreted by cells in the brain, injury of the brain could be prevented. To examine the possibility of long-term cell treatment of the brain in LSDs, we carried out a transplantation experiment in the brain of a GM1-gangliosidosis mouse model (acid β-galactosidase knock-out mouse) using fetal brain cells (FBC) and mesenchymal stem cells (MSC) from bone marrow. These cells used for transplantation were derived from mice of the same genetic background as recipient mice except for possession of the human β-galactosidase gene.

2. Materials and methods

2.1. Knock-out and transgenic mice

A mouse model of GM1 gangliosidosis (BKO mouse) was generated by targeting of the β-galactosidase gene at exon 15 in ES cells as previously described [23]. Newborn mice were obtained by mating heterozygous female mice with homozygous male mice. Identification of newborn mutants was accomplished by quantitative analysis of β-galactosidase activity in tail tip homogenates on the day of birth. Mice with high β-galactosidase activity (TG mice) [24] were generated by introducing the human β-galactosidase gene as a transgene in ES cells obtained from the BKO mouse, which has several copies of the human β-galactosidase gene without the mouse β-galactosidase background. Age-matched wild-type mice of C57BL/6 strain were used as a control.

2.2. Cell preparations for transplantation

Cultured mesenchymal stem cells (MSC) were obtained from the bone marrow of the tibias and femurs of 5–8 month-old TG mice according to the method of Meirelles et al. [25] with some modifications. Dulbecco's modified Eagle's medium (DMEM: Sigma Chemical Co., St Louis, MO) containing 10% fetal bovine serum (Medical and Biological Laboratories, Nagoya, Japan) was used for culture.

Fetal brain cells (FBC) were obtained from the fetal cerebral cortex of TG mice at 13 days of gestation according to the method of Meberg and Miller [26]. The brain tissue was disrupted in a Pasteur glass pipette by gentle stroking several times (uncultured FBC), and then cultured for 4 h in Neurobasal medium (Invitrogen, Carlsbad, CA, No. 12348-07) containing 2 mM glutamine and 10% FBS, followed by two days in Neurobasal medium containing 2 mM glutamine and B27 supplement (Invitrogen, No. 14175-095) (cultured FBC).

2.3. Transplantation of cells into newborn mouse brain

Each BKO mouse received a single injection of 0.5–1.0×10^5 of the cells prepared as described above in the right cerebral ventricle from 24 to 48 hours after birth. Study groups were as follows: uncultured FBC ($n = 18$), cultured FBC ($n = 10$), MSC ($n = 17$), and mixed MSC and FBC (1:1) ($n = 15$). Mice of each experimental group were divided into three subgroups for X-gal staining, β-galactosidase assay and ganglioside GM1 analysis. Mice were examined at one, two, four, and eight weeks and 6 months after injection as shown in Table 1.

For biochemical analysis, mice were anesthetized with diethylether and the blood was washed out with normal saline by perfusion through the heart, and the

brains were removed and kept at −80 °C until use. For histological studies, the brains were fixed by perfusion through the heart with 4% paraformaldehyde in 0.1 M phosphate buffer pH 7.4 (PB) for 20 min., after washing out the blood with normal saline. To obtain frozen sections, the brains were placed in 0.1 M phosphate buffer pH 7.4 containing 30% sucrose, and frozen in liquid nitrogen.

All surgical and care procedures were carried out in accordance with the Guidelines for Use and Care of Experimental Animals approved by the Animal Committee of Osaka City University School of Medicine.

2.4. X-Gal staining

Frozen sections (16 μm thick) were reacted with X-gal using the β-gal staining Kit (Invitrogen Corp., Carlsbad, CA) to visualize β-galactosidase activity.

2.5. β-Galactosidase assay

β-Galactosidase activity was analyzed in the tissue homogenate with the artificial substrate 2 mM 4-methylumbelliferyl β-galactoside at pH 4.0 in 0.1 M sodium citrate-phosphate buffer according to the method described by Suzuki [27]. Protein was analyzed using the Bio-Rad protein assay system (Bio-Rad Laboratories, Hercules, CA) with the method of Bradford [28].

2.6. Analysis of ganglioside GM1

Amounts of ganglioside GM1 were measured by immunoblot assay using anti-GM1 ganglioside monoclonal antibody (Code: 370685, Seikagaku Corp., Tokyo, Japan) by the method of Michikawa et al. [29] with some modifications.

Brain tissue cells were disrupted by sonication and solubilized in 20 mM Tris–HCl buffer pH 8.0 containing 137 mM NaCl, 10% glycerol, and a protease inhibitor cocktail (Complete, Mini, Cat No. 11836153001, Roche Diagnostics, Mannheim, Germany). Five micrograms of tissue protein was applied onto Trans-Blot Transfer Medium Pure Nitrocellulose Membrane (0.45 μm pore size, Code: 162-0117, Bio-Rad Laboratories) through the slots of a Bio-Dot SF Microfiltration Apparatus (Bio-Rad Laboratories). The membrane was reacted with anti-GM1 ganglioside monoclonal antibody diluted 1:500, after blocking with 5% skim milk in PBS solution for 1 h at room temperature, and then with horseradish peroxidase-linked anti-mouse IgG sheep antibody (Code: NA931, GE Healthcare UK Ltd., Buckinghamshire, UK) diluted 1:1,000. The washing solution used was 0.1 M Tris buffered saline pH 7.5 containing 0.1% Tween 20 (TTBS). Bound antibody was detected using ECL after reaction with ECL™ Western Blotting Detection Reagents (Code: RPN2209, GE Healthcare UK Ltd.) and visualized on X-ray film. Densitometric quantification of immunoreactive signal was performed using the Kodak Digital Science™ EDAS 120 system with 1D Image Analysis software (Eastman Kodak Company, NY). The values obtained were compared with those of quantification of histological immunoreactivity with Leica Control Software as previously described [30], and the same ratios were obtained among the samples (data not shown). The assay was performed three times and in duplicate for each sample independently, and mean values were calculated.

3. Results

3.1. X-Gal staining

Layered staining of the transplanted cells was observed over the entire ventricular surface on both sides of the cerebral hemispheres in treated mice at one week after injection (data not shown). Positive cells had spread into the brain tissue by two weeks (Fig. 1c and f) in the mice treated with cultured FBC ($n = 1$), uncultured FBC ($n = 1$), and MSC ($n = 2$) in the same amounts. The cells had spread further and had reached every part of the brain by 4 weeks in the mice of all experimental groups (Fig. 1d, g and i). Less positive cells were found in the mice treated with MSC ($n = 3$) or mixed MSC and FBC ($n = 3$) (Fig. 1g and i) than in the mice treated with cultured ($n = 3$) or uncultured FBC ($n = 3$) (Fig. 1d). The number of the X-Gal positive cells increased gradually until 4 weeks after injection in every experimental mouse. At 8 weeks after injection, positive cells still existed in the cultured FBC- ($n = 3$) and uncultured FBC-treated ($n = 3$) mice (Fig. 1e) in the same numbers with a similar distribution as at 4 weeks. However, a significant decrease in number of positive cells was found at 8 weeks in the mice treated with MSC ($n = 3$) or mixed MSC and FBC ($n = 3$) (Fig. 1h and j). In the mice treated with mixed MSC and FBC, positive cells existed in higher numbers in deep areas than in the mice treated with MSC alone. In the mice treated with cultured ($n = 2$) and uncultured FBC ($n = 2$), small numbers of positive cells with strong staining still existed in many parts of the brain, especially around the striatum and lateral globs pallidus (Fig. 1k and l), at 6 months after injection. No grafted cells were found in the mice treated with MSC ($n = 1$) or mixed MSC and FBC ($n = 1$) at 6 months. No significant differences were noted among the mice within each experimental group at each stage.

3.2. β-Galactosidase activity

The β-galactosidase activity in FBC and MSC derived from TG mice were 214.5–227.5 nmol/mg/h ($n = 4$) and 143.0–121.4 nmol/mg/h ($n = 3$), respec-

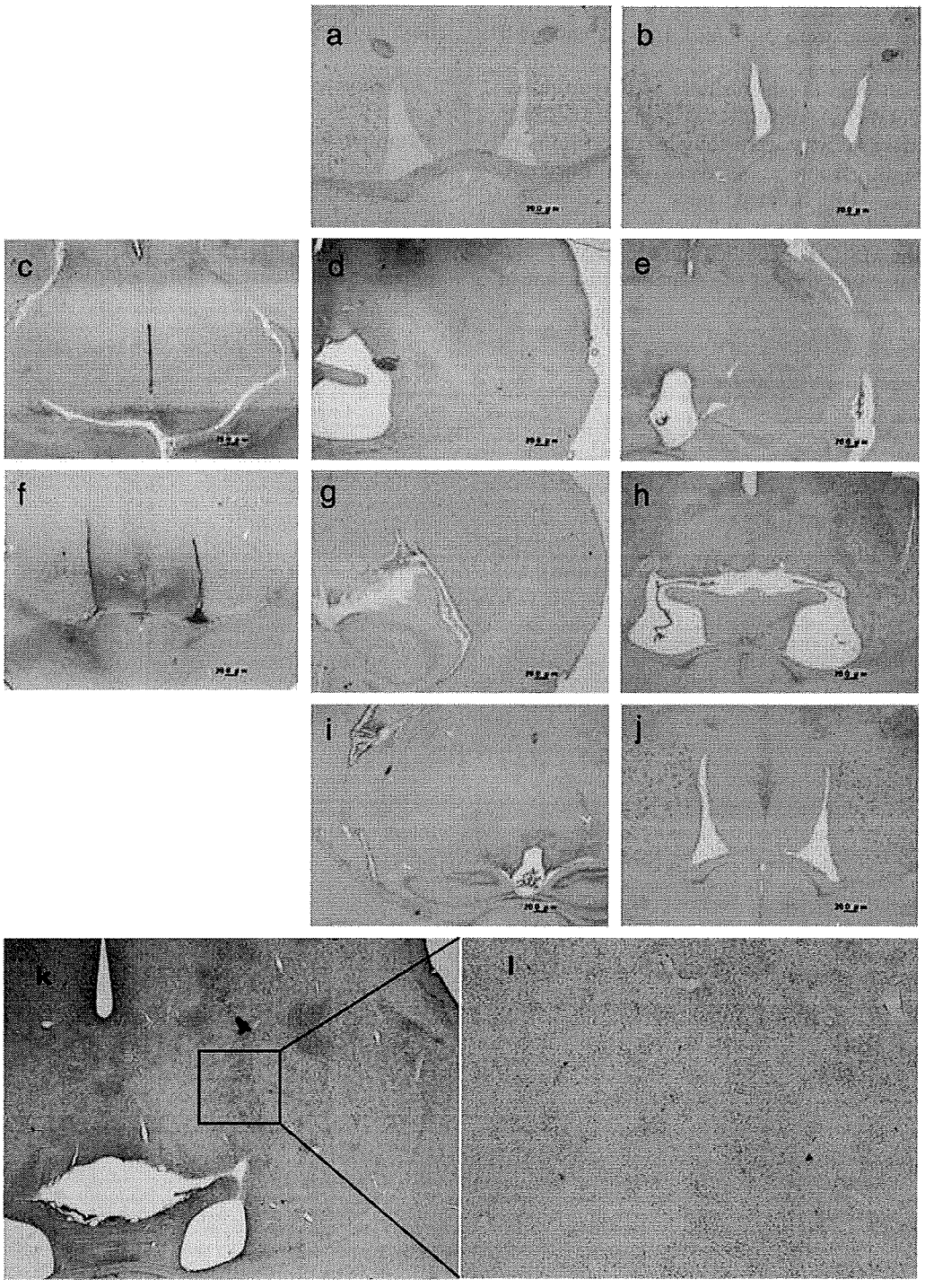

Fig. 1. X-Gal staining of brain coronal sections at +0.8 mm to −2.0 mm of bregma. (a and b) Non-treated BKO mouse at 4 and 8 weeks old, respectively; (c–e) Treated with FBC at 2, 4, and 8 weeks after injection; (f–h) Treated with MSC at 2, 4, and 8 weeks after injection; (i and j) Treated with mixed MSC and FBC at 4 and 8 weeks after injection; (k) FBC-treated brain at 6 months after injection; (l) Magnification of figure k. Positive cells had spread into the brain tissue by two weeks (c and f). The cells had spread further by 4 weeks (d, g and i). Less positive cells were found in the mice treated with MSC or mixed MSC and FBC (g and i) than in the mice treated with FBC (d). At 8 weeks, positive cells still existed in FBC-treated mouse (e) as at 4 weeks (d). A significant decrease in number of positive cells was found at 8 weeks in the mice treated with MSC (h) or mixed MSC and FBC (j). Strong positive staining cells still existed at 6 months in the brain of FBC-treated mouse (k and l).

tively, while the activity in FBC and in MSC derived from wild-type mice were 54.9–69.1 ($n = 2$) and 63.0 ($n = 1$), respectively.

The results of brain β-galactosidase activity in transplantation experiments are shown in Table 2. Increases in β-galactosidase activity were found in the brains of each experimental group at 4 weeks after injection. Activity in the FBC-treated mice was definitely increased at 4 weeks as well as at 8 weeks, while activity at 8 weeks in the MSC-treated mice and mixed MSC and FBC-treated mice was almost the same level as that in the untreated mice. These findings were consistent with those in the X-Gal staining study.

3.3. Immunoassay of ganglioside GM1

Immunoassay of accumulated ganglioside GM1 was performed for each mouse using anti-GM1 ganglioside monoclonal antibody. Values are ratios to the amounts in age-matched normal control mice. The results are shown in Fig. 2 and Tables 3. At 4 weeks after injection, remarkable decrease in ganglioside GM1 accumulation

Table 1
Mouse numbers used for each experiment.

Time after injection	1 week	2 weeks	4 weeks	8 weeks	6 months
	[X-Gal staining]				
Uncultured FBC	1	1	3	3	2
Cultured FBC	1	1	3	3	2
MSC		2	3	3	1
Mixed MSC and FBC			3	3	1
	[β-galactosidase activity]				
Uncultured FBC			2	2	
Cultured FBC					
MSC			2	2	
Mixed MSC and FBC			2	2	
	[Immunoblot assay of ganglioside GM1 amount]				
Uncultured FBC			1	1	1
Cultured FBC					
MSC			2	2	
Mixed MSC and FBC			2	2	

Table 2
β-Galactosidase activity.

	4 weeks	8 weeks
Age-matched normal control (mean ± SD)	197 ± 61 ($n = 7$)	159 ± 56 ($n = 7$)
Non-treated (mean ± SD)	4.38 ± 0.35 ($n = 5$)	4.10 ± 0.47 ($n = 5$)
Treated with uncultured FBC	Mouse 1	Mouse 7
	Rt: 6.65[a]	Rt: 4.94
	Lt: 5.31[a]	Lt: 6.03[a]
	Mouse 2	Mouse 8
	Rt: 7.36[a]	Rt: 5.58[a]
	Lt: 5.33[a]	Lt: 5.05[a]
Treated with MSC	Mouse 3	Mouse 9
	Rt: 6.30[a]	Rt: 4.13
	Lt: 5.95[a]	Lt: 3.67
	Mouse 4	Mouse 10
	Rt: 5.74[a]	Rt: 4.19
	Lt: 5.12[a]	Lt: 5.05[a]
Treated with mixed MSC and FBC	Mouse 5	Mouse 11
	Rt: 5.80[a]	4.13 (mix of both hemispheres)
	Lt: 5.40[a]	
	Mouse 6	Mouse 12
	Rt: 5.06	Rt: 4.85
	Lt: 4.52	Lt: 5.02

Values are in nmol/mg/h. Each sample was tested in duplicate and results are mean values. Rt, right hemisphere; Lt, left hemisphere.
[a] Increase of activity over mean + 2SD of non-treated mice.

Table 3
Immunoblot assay of ganglioside GM1 amount.

	4 weeks	8 weeks	6 months
Age-matched non-treated (range)	2.65–3.55 ($n = 3$)	4.98–5.28 ($n = 3$)	7.58 (n = 1)
Treated with uncultured FBC	Mouse I	Mouse VI	Mouse XI
	Rt: 1.42[a]	Rt: 2.30[a]	Rt: 6.18[b]
	Lt: 1.80[a]	Lt: 2.44[a]	Lt: 6.40[b]
Treated with MSC	Mouse II	Mouse VII	
	Rt: 1.82[a]	Rt: 5.30	
	Lt: 1.31[a]	Lt: 5.23	
	Mouse III	Mouse VIII	
	Rt: 1.40[a]	Rt: 4.40[b]	
	Lt: 1.34[a]	Lt: 4.73[b]	
Treated with mixed MSC and FBC	Mouse IV	Mouse IX	
	Rt: 1.33[a]	Rt: 4.55[b]	
	Lt: 1.34[a]	Lt: 4.78[b]	
	Mouse V	Mouse X	
	Rt: 1.78[a]	Rt: 4.45[b]	
	Lt: 1.62[a]	Lt: 4.58[b]	

Values are ratios to those for age-matched control mice. Each sample was tested in duplicate for three times and results are mean values. Rt, right hemisphere; Lt, left hemisphere.
[a] Remarkable decrease.
[b] Slight decrease of ganglioside GM1 compared with non-treated mice.

was found in the mice of every group. However, at 8 weeks, decrease was detected only in the mouse treated with FBC. Efficacy was still noted at 6 months after injection in FBC-treated mouse. These findings were consistent with those for X-Gal staining (Fig. 1) and β-galactosidase activity (Table 2).

4. Discussion

Two therapeutic methods, HSCT and ERT, are clinically available for LSDs. However, neither is markedly effective in the brain. A number of experiments in animal models have been carried out on the treatment of brain in LSDs. Each revealed some efficacy in the brain, though it was transient and incomplete. Sufficient enzyme expression throughout life is needed in the brain. Thus, permanent engraftment of enzyme-secreting cells in the brain, or permanent expression of an exogenous gene with a vector or as an integrated gene might eliminate the brain involvement in LSDs.

However, the immune responses of host animals are among the most difficult problems to overcome in this respect [31–33]. Although the brain, which is sequestered from systemic immune responses, is thought to exhibit little immune response, elimination of cells expressing a therapeutic transgene occurs in the brain. We speculate that innate inflammatory immune responses are stimulated to kill such cells, not necessarily with the induction of a linked adaptive immune response. When host brain cells express a therapeutic transgene mediated by a viral vector, the host cells themselves will be eliminated, possibly resulting in acceleration of neuronal cell death in neurodegenerative disorders. Transplantation of cells having the same genetic information as the host animals with LSD except for expression of a deficient enzyme protein would thus be a good method of treatment for avoiding the elimination of host neuronal cells and curing diseased host cells.

We performed cell transplantation into the brain of β-galactosidase-deficient mice to study the usefulness of long-term engraftment for supplementation of deficient enzyme protein. To minimize the immune responses in the recipient β-galactosidase knock-out mice, we used cells of mice with the same genetic background as the recipient except for possession of copies of the human β-galactosidase gene.

Initially, in the transplantation experiment, we used FBC from transgenic mice expressing the human β-galactosidase gene. The cells could grow in an environment similar to that of the recipient organ in which they were originally growing. The cells spread into the brains and the cell number increased at least until 4 weeks. They grew very successfully for at least 8 weeks and survived for 6 months or more. However, the number of engrafted cells had decreased significantly at 6 months, while the size of the brain had increased. The decrease in ganglioside GM1 accumulation was also marked until 8 weeks after transplantation. However, at 6 months, this decrease was far less pronounced, with re-accumulation of ganglioside GM1. After the cells were engrafted and the cell number was increased by the cell division in the recipient brain, they were depleted. The mechanism of depletion of transplanted cells involved immunological rejection, although the transplanted cells were very similar genetically and physiologically to the recipient.

Next, we performed a transplantation experiment using MSCs obtained from the bone marrow of the

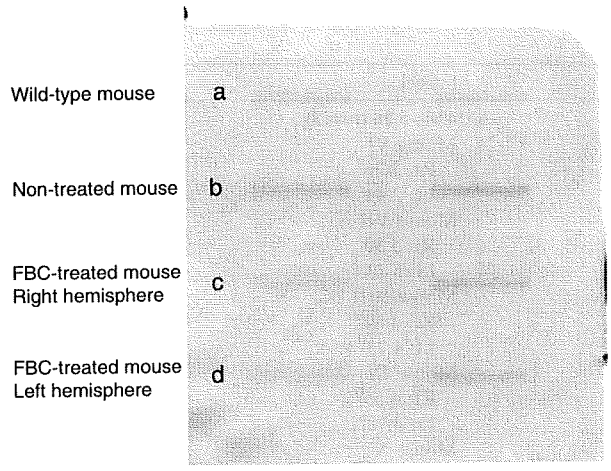

Fig. 2. Immunoblot assay of ganglioside GM1 in brain homogenate at 8 weeks after treatment. Performed in duplicate as shown in two slots for each sample. (a) Wild-type mouse; (b) Non-treated mouse; (c and d) Right and left hemisphere, respectively, of a mouse treated with FBC. The immunoreactivity against ganglioside GM1 antibody in the treated brain (c and d) was less than non-treated brain (d). The accumulated amounts of ganglioside GM1 were calculated in the ratio to the age-matched wild-type mouse (a) from the densitometric quantification signals. These values were shown in Table 3.

same mice expressing the human β-galactosidase gene. MSCs were obtained using the method of plastic adherence. This relatively crude procedure produces a heterogeneous population including multipotential MSCs. These crude cells were used to avoid depletion of potentially important cells and for ease of preparation for clinical application. The cells spread into the brains and the cell number increased similarly to FBC transplantation experiment until 4 weeks. However, decrease in number of engrafted living cells and efficacy in preventing accumulation of ganglioside GM1 were observed in the examination of 8-week-old treated mice.

A number of studies on neural transdifferentiation have been reported [34–37]. Some have reported that neural transdifferentiation of MSCs is induced by cell fusion with host neuronal cells [38–41]. We therefore used mixed FBC and MSC cells to stimulate cell fusion. More engrafted cells were found in the deep areas of the mouse brains treated with mixed cells than in the brains treated with MSC alone. However, no fused cells could be identified. The long-living cells were probably transplanted FBC themselves.

Decrease of ganglioside GM1 was observed even though the increase of the β-galactosidase activity was so small. Similar efficacy was shown previously in our gene therapy experiment [2]. On the other hand, we observed a general depletion of the transplanted cells over time in the BKO mouse brains. The transplanted cells survived in early stage and the number increased by cell division, then, died. This was likely caused by immunological rejection, even though we used fetal brain cells (FBC) from mice with the same genetic background for transplantation. We speculated that immunological reaction occurred because these cells expressed the therapeutic enzyme protein which the host animals did not have. The same has been reported in the transplantation of autogenous cells expressing an exogenous therapeutic gene [33]. The grafted cells were gradually depleted because of immunological rejection by the host animals. To avoid deleterious immune attack and to achieve sufficient long-term efficacy in brain, development of methods to steer the immune response away from cytotoxic responses or to induce tolerance to the products of therapeutic genes is needed [42,43].

Acknowledgements

We thank Kaoru Takano and Takanori Kunieda for mating of mice and providing the BKO and TG mice in timely fashion for each experiment.

This work was supported by grant AT-18591163 from the Ministry of Education, Culture, Sports, Science, and Technology of Japan.

References

[1] Shen JS, Watabe K, Ohashi T, Eto Y. Intraventricular administration of recombinant adenovirus to neonatal twitcher mouse leads to clinicopathological improvements. Gene Ther 2001;8:1081–7.

[2] Takaura N, Yagi T, Maeda M, Nanba E, Oshima A, Suzuki Y, et al. Attenuation of ganglioside GM1 accumulation in the brain of GM1 gangliosidosis mice by neonatal intravenous gene transfer. Gene Ther 2003;10:1487–93.

[3] Kim EY, Hong YB, Lai Z, Cho YH, Brady RO, Jung SC. Long-term expression of the human glucocerebrosidase gene in vivo after transplantation of bone-marrow-derived cells transformed with a lentivirus vector. J Gene Med 2005;7:878–87.

[4] Shen JS, Meng XL, Yokoo T, Sakurai K, Watabe K, Ohashi T, et al. Widespread and highly persistent gene transfer to the CNS by retrovirus vector in utero: implication for gene therapy to Krabbe disease. J Gene Med 2005;7:540–51.

[5] Cachón-González MB, Wang SZ, Lynch A, Ziegler R, Cheng SH, Cox TM. Effective gene therapy in an authentic model of Tay-Sachs-related diseases. Proc Natl Acad Sci USA 2006;103:10373–8.

[6] Kopen GC, Prockop DJ, Phinney DG. Marrow stromal cells migrate throughout forebrain and cerebellum, and they differentiate into astrocytes after injection into neonatal mouse brains. Proc Natl Acad Sci USA 1999;96:10711–6.

[7] Jin HK, Carter JE, Huntley GW, Schuchman EH. Intracerebral transplantation of mesenchymal stem cells into acid sphingomyelinase-deficient mice delays the onset of neurological abnormalities and extends their life span. J Clin Invest 2002;109:1183–91.

[8] Sakurai K, Iizuka S, Shen JS, Meng XL, Mori T, Umezawa A, et al. Brain transplantation of genetically modified bone marrow stromal cells corrects CNS pathology and cognitive function in MPS VII mice. Gene Ther 2004;11:1475–81.

[9] Givogri MI, Galbiati F, Fasano S, Amadio S, Perani L, Superchi D, et al. Oligodendroglial progenitor cell therapy limits central

neurological deficits in mice with metachromatic leukodystrophy. J Neurosci 2006;26:3109–19.
[10] Kakkis E, McEntee M, Vogler C, Le S, Levy B, Belichenko P, et al. Intrathecal enzyme replacement therapy reduces lysosomal storage in the brain and meninges of the canine model of MPS I. Mol Genet Metab 2004;83:163–74.
[11] Dickson P, McEntee M, Vogler C, Le S, Levy B, Peinovich M, et al. Intrathecal enzyme replacement therapy: successful treatment of brain disease via the cerebrospinal fluid. Mol Genet Metab 2007;91:61–8.
[12] Vogler C, Levy B, Grubb JH, Galvin N, Tan Y, Kakkis E, et al. Overcoming the blood–brain barrier with high-dose enzyme replacement therapy in murine mucopolysaccharidosis VII. Proc Natl Acad Sci USA 2005;102:14777–82.
[13] Matzner U, Herbst E, Hedayati KK, Lüllmann-Rauch R, Wessig C, Schröder S, et al. Enzyme replacement improves nervous system pathology and function in a mouse model for metachromatic leukodystrophy. Hum Mol Genet 2005;14:1139–52.
[14] Blanz J, Stroobants S, Lüllmann-Rauch R, Morelle W, Lüdemann M, D'Hooge R, et al. Reversal of peripheral and central neural storage and ataxia after recombinant enzyme replacement therapy in {alpha}-mannosidosis mice. Hum Mol Genet 2008;17:3437–45.
[15] Grubb JH, Vogler C, Levy B, Galvin N, Tan Y, Sly WS. Chemically modified {beta}-glucuronidase crosses blood–brain barrier and clears neuronal storage in murine mucopolysaccharidosis VII. Proc Natl Acad Sci USA 2008;105:2616–21.
[16] Montaño AM, Oikawa H, Tomatsu S, Nishioka T, Vogler C, Gutierrez MA, et al. Acidic amino acid tag enhances response to enzyme replacement in mucopolysaccharidosis type VII mice. Mol Genet Metab 2008;94:178–89.
[17] Kasperzyk JL, El-Abbadi MM, Hauser EC, D'Azzo A, Platt FM, Seyfried TN. *N*-butyldeoxygalactonojirimycin reduces neonatal brain ganglioside content in a mouse model of GM1 gangliosidosis. J Neurochem 2004;89:645–53.
[18] Lachmann RH, te Vruchte D, Lloyd-Evans E, Reinkensmeier G, Sillence DJ, Fernandez-Guillen L, et al. Treatment with miglustat reverses the lipid-trafficking defect in Niemann-Pick disease type C. Neurobiol Dis 2004;16:654–8.
[19] Cox TM. Substrate reduction therapy for lysosomal storage diseases. Acta Paediatr Suppl. 2005;94:69–75.
[20] Piotrowska E, Jakóbkiewicz-Banecka J, Barańska S, Tylki-Szymańska A, Czartoryska B, Wegrzyn A, et al. Genistein-mediated inhibition of glycosaminoglycan synthesis as a basis for gene expression-targeted isoflavone therapy for mucopolysaccharidoses. Eur J Hum Genet 2006;14:846–52.
[21] Ishii S, Yoshioka H, Mannen K, Kulkarni AB, Fan JQ. Transgenic mouse expressing human mutant alpha-galactosidase A in an endogenous enzyme deficient background: a biochemical animal model for studying active-site specific chaperone therapy for Fabry disease. Biochim Biophys Acta 2004;1690:250–7.
[22] Matsuda J, Suzuki O, Oshima A, Yamamoto Y, Noguchi A, Takimoto K, et al. Chemical chaperone therapy for brain pathology in G(M1)-gangliosidosis. Proc Natl Acad Sci USA 2003;100:15912–7.
[23] Matsuda J, Suzuki O, Oshima A, Ogura A, Noguchi Y, Yamamoto Y, et al. Beta-galactosidase-deficient mouse as an animal model for GM1-gangliosidosis. Glycoconj J 1997;14:729–36.
[24] Yamamoto Y, Nagase Y, Noguchi A, Mochida K, Nakahira M, Takano K, et al. Generation and characterization of the β-galactosidase knockout mouse having the normal human β-galactosidase gene as a transgene (in Japanese). Proc Jap Soc of Animal Models for Hum Dis (Nippon Shikkan Model Gakkai Kiroku) 2001;17:20–2.
[25] Meirelles Lda S, Nardi NB. Murine marrow-derived mesenchymal stem cell: isolation, in vitro expansion, and characterization. Br J Haematol 2003;123:702–11.
[26] Meberg PJ, Miller MW. Culturing hippocampal and cortical neurons. Methods Cell Biol 2003;71:111–27.
[27] Suzuki K. Enzymatic diagnosis of sphingolipidosis. Methods Enzymol 1987;138:727–62.
[28] Bradford MM. A Rapid and sensitive method for the quantitation of microgram quantities of protein utilizing the principle of protein-dye binding. Anal Biochem 1976;72:255–60.
[29] Michikawa M, Gong JS, Fan QW, Sawamura N, Yanagisawa K. A novel action of alzheimer's amyloid beta-protein (Abeta): oligomeric Abeta promotes lipid release. J Neurosci 2001;21:7226–35.
[30] Suzuki Y, Ichinomiya S, Kurosawa M, Ohkubo M, Watanabe H, Iwasaki H, et al. Chemical chaperone therapy: clinical effect in murine G(M1)-gangliosidosis. Ann Neurol 2007;62:671–5.
[31] Barker RA, Widner H. Immune problems in central nervous system cell therapy. NeuroRx 2004;1:472–81.
[32] Abordo-Adesida E, Follenzi A, Barcia C, Sciascia S, Castro MG, Naldini L, et al. Stability of lentiviral vector-mediated transgene expression in the brain in the presence of systemic antivector immune responses. Hum Gene Ther 2005;16:741–51.
[33] Lowenstein PR, Kroeger K, Castro MG. Immunology of neurological gene therapy: how T cells modulate viral vector-mediated therapeutic transgene expression through immunological synapses. Neurotherapeutics 2007;4:715–24.
[34] Weimann JM, Charlton CA, Brazelton TR, Hackman RC, Blau HM. Contribution of transplanted bone marrow cells to Purkinje neurons in human adult brains. Proc Natl Acad Sci USA 2003;100:2088–93.
[35] Abouelfetouh A, Kondoh T, Ehara K, Kohmura E. Morphological differentiation of bone marrow stromal cells into neuron-like cells after co-culture with hippocampal slice. Brain Res 2004;1029:114–9.
[36] Wislet-Gendebien S, Hans G, Leprince P, Rigo JM, Moonen G, Rogister B. Plasticity of cultured mesenchymal stem cells: switch from nestin-positive to excitable neuron-like phenotype. Stem cells 2005;23:392–402.
[37] Deng J, Petersen BE, Steindler DA, Jorgensen ML, Laywell ED. Mesenchymal stem cells spontaneously express neural proteins in culture and are neurogenic after transplantation. Stem cells 2006;24:105410–64.
[38] Terada N, Hamazaki T, Oka M, Hoki M, Mastalerz DM, Nakano Y, et al. Bone marrow cells adopt the phenotype of other cells by spontaneous cell fusion. Nature 2002;416:542–5.
[39] Alvarez-Dolado M, Pardal R, Garcia-Verdugo JM, Fike JR, Lee HO, Pfeffer K, et al. Fusion of bone-marrow-derived cells with Purkinje neurons, cardiomyocytes and hepatocytes. Nature 2003;425:968–73.
[40] Kozorovitskiy Y, Gould E. Stem cell fusion in the brain. Nat Cell Biol 2003;5:952–4.
[41] Bae JS, Furuya S, Shinoda Y, Endo S, Schuchman EH, Hirabayashi Y, et al. Neurodegeneration augments the ability of bone marrow-derived mesenchymal stem cells to fuse with Purkinje neurons in Niemann-Pick type C mice. Hum Gene Ther 2005;16:1006–11.
[42] Tomatsu S, Gutierrez M, Nishioka T, Yamada M, Yamada M, Tosaka Y, et al. Development of MPS IVA mouse (Galnstm(hC79S. mC76S)slu) tolerant to human *N*-acetylgalactosamine-6-sulfate sulfatase. Hum Mol Genet 2005;14:3321–5.
[43] Matzner U, Matthes F, Herbst E, Lüllmann-Rauch R, Callaerts-Vegh Z, D'Hooge R, et al. Induction of tolerance to human arylsulfatase A in a mouse model of metachromatic leukodystrophy. Mol Med 2007;13:471–9.

THE JOURNAL OF BIOLOGICAL CHEMISTRY VOL. 284, NO. 9, pp. 5592–5601, February 27, 2009
Printed in the U.S.A.

Angiopoietin-1 Induces Krüppel-like Factor 2 Expression through a Phosphoinositide 3-Kinase/AKT-dependent Activation of Myocyte Enhancer Factor 2*[S]◆

Received for publication, September 8, 2008, and in revised form, November 24, 2008 Published, JBC Papers in Press, December 23, 2008, DOI 10.1074/jbc.M806928200

Keisuke Sako[‡], Shigetomo Fukuhara[‡1], Takashi Minami[§], Takao Hamakubo[§], Haihua Song[§], Tatsuhiko Kodama[§], Akiyoshi Fukamizu[¶], J. Silvio Gutkind[‖], Gou Young Koh[**], and Naoki Mochizuki[‡]

*From the [‡]Department of Structural Analysis, National Cardiovascular Center Research Institute, 5-7-1 Fujishirodai, Suita, Osaka 565-8565, Japan, the [§]Laboratory for System Biology and Medicine, Research Center for Advanced Science and Technology, University of Tokyo, 4-6-1, Komaba, Meguro, Tokyo 153-8904, Japan, the [¶]Center for Tsukuba Advanced Research Alliance, University of Tsukuba, Tsukuba, Ibaraki 305-8577, Japan, the [‖]Oral and Pharyngeal Cancer Branch, NIDCR, National Institutes of Health, Bethesda, Maryland 20892, and the **Biomedical Research Center and Department of Biological Sciences, Korea Advanced Institute of Science and Technology, Guseong-dong, Daejeon 305-701, Korea*

Angiopoietin-1 (Ang1) regulates both vascular quiescence and angiogenesis through the receptor tyrosine kinase Tie2. We and another group have recently shown that Ang1 and Tie2 form distinct signaling complexes at cell-cell and cell-matrix contacts and further demonstrated that the former selectively induces expression of Krüppel-like factor 2 (KLF2), a transcription factor involved in vascular quiescence. Here, we investigated the mechanism of how Ang1/Tie2 signal induces KLF2 expression to clarify the role of KLF2 in Ang1/Tie2 signal-mediated vascular quiescence. Ang1 stimulated KLF2 promoter-driven reporter gene expression in endothelial cells, whereas it failed when a myocyte enhancer factor 2 (MEF2)-binding site of KLF2 promoter was mutated. Depletion of MEF2 by siRNAs abolished Ang1-induced KLF2 expression, indicating the requirement of MEF2 in KLF2 induction by Ang1. Constitutive active phosphoinositide 3-kinase (PI3K) and AKT increased the MEF2-dependent reporter gene expression by enhancing its transcriptional activity and stimulated the KLF2 promoter activity cooperatively with MEF2. Consistently, inhibition of either PI3K or AKT and depletion of AKT abrogated Ang1-induced KLF2 expression. In addition, we confirmed the dispensability of extracellular signal-regulated kinase 5 (ERK5) for Ang1-induced KLF2 expression. Furthermore, depletion of KLF2 resulted in the loss of the inhibitory effect of Ang1 on vascular endothelial growth factor (VEGF)-mediated expression of vascular cell adhesion molecule-1 in endothelial cells and VEGF-mediated monocyte adhesion to endothelial cells. Collectively, these findings indicate that Ang1/Tie2 signal stimulates transcriptional activity of MEF2 through a PI3K/AKT pathway to induce KLF2 expression, which may counteract VEGF-mediated inflammatory responses.

Angiopoietin-1 (Ang1)[2] is a ligand for endothelium-specific receptor tyrosine kinase Tie-2. Gene-targeting analyses of either *Ang1* or *Tie2* in mice reveal an essential role of Ang1/Tie2 signaling in developmental vascular formation (1–3). In adult vasculature, Ang1/Tie2 signal maintains quiescence of mature blood vessels by enhancing vascular integrity and endothelial survival (4–6). However, Tie2 signaling is also involved in physiological and pathological angiogenesis, as opposed to the maintenance of vascular quiescence (4, 5, 7–9). As to this question, we and Alitalo's group (10, 11) have recently clarified that the distinct localization of Tie2 in the presence or absence of cell-cell contact determines the specificity of downstream signaling of Tie2. Ang1 induces *trans*-association of Tie2 at endothelial cell-cell contacts, whereas Tie2 is anchored to extracellular matrix by Ang1 in the absence of cell-cell contacts. *Trans*-associated Tie2 bridged by Ang1 and extracellular matrix-anchored Tie2 by Ang1 induce distinct signaling pathways preferable for vascular quiescence and angiogenesis via AKT and extracellular signal-regulated kinase (ERK) 1/2, respectively. By performing DNA microarray analysis, we also revealed that a distinct set of genes is regulated by Ang1 in the presence or absence of cell-cell contacts. Among them, Krüp-

* This work was supported by grants from the Ministry of Education, Science, Sports and Culture of Japan (to K. S., S. F., and N. M.); the Ministry of Health, Labour, and Welfare of Japan (to N. M.); and the Program for the Promotion of Fundamental Studies in Health Sciences of the National Institute of Biomedical Innovation (to S. F., T. M., T. K., and N. M.); the Naito Foundation (to S. F.); Takeda Science Foundation (to S. F.); the Sagawa Foundation for Promotion of Cancer Research (to S. F.), Mochida Memorial Foundation for Medical and Pharmaceutical Research (to S. F.), Kowa Life Science Foundation (to S. F.), Kanae Foundation for the Promotion of Medical Science (to S. F.), and Takeda Medical Research Foundation (to N. M.). The costs of publication of this article were defrayed in part by the payment of page charges. This article must therefore be hereby marked "*advertisement*" in accordance with 18 U.S.C. Section 1734 solely to indicate this fact.
◆ This article was selected as a Paper of the Week.
[S] The on-line version of this article (available at http://www.jbc.org) contains five supplemental figures.
[1] To whom correspondence should be addressed. Tel.: 81-6-6833-5012; Fax: 81-6-6835-5461; E-mail: fuku@ri.ncvc.go.jp.

[2] The abbreviations used are: Ang1, angiopoietin-1; KLF2, Krüppel-like factor 2; COMP, cartilage oligomeric matrix protein; MEF2, myocyte enhancer factor 2; ERK, extracellular signal-regulated kinase; PI3K, phosphoinositide 3-kinase; VEGF, vascular endothelial growth factor; VEGFR2, VEGF receptor 2; VCAM-1, vascular cell adhesion molecule-1; GFP, green fluorescent protein; GST, glutathione *S*-transferase; HUVEC, human umbilical vein endothelial cell; RT, reverse transcription; GAPDH, glyceraldehyde-3-phosphate dehydrogenase; HDAC, histone deacetylase; PCAF, p300/CBP-associated factor; CBP, CREB-binding protein; CREB, cAMP-response element-binding protein; BSA, bovine serum albumin; siRNA, small interfering RNA; MOPS, 4-morpholinepropanesulfonic acid; wt, wild type; mut, mutant; Luc, luciferase; CA, constitutive active.

pel-like factor 2 (KLF2) was selectively induced by Ang1 in the presence of cell-cell contacts (10).

KLF2 is a zinc finger family of transcription factor functioning in both vascular smooth muscle cells and endothelial cells and is, therefore, essential in developmental vascular formation (12–15). The *KLF2* knock-out mice exhibit impaired blood vessel formation attributable to the lack of smooth muscle cell recruitment (12). KLF2 expression in endothelium is induced by laminar shear stress and is thought to act as a molecular transducer of laminar shear stress (16–18). In the adult human vasculature, KLF2 expression is found at laminar segments of blood vessels and is decreased at branched points, which are more prone to develop atherosclerotic lesions (18), suggesting the role of KLF2 as a flow-mediated atheroprotective factor. Consistently, more than 15% of flow-regulated genes are dependent upon flow-mediated KLF2 induction (19).

It has been reported that laminar shear stress induces KLF2 expression via an ERK5-myocyte enhancer factor 2 (MEF2) signaling pathway (19, 20). The MEF2 family of transcription factors is composed of four members (MEF2A, MEF2B, MEF2C, and MEF2D) and is known as a regulator of vascular functions (21–23). Therefore, KLF2 may act downstream of MEF2 to regulate vascular functions.

KLF2 controls endothelial functions by negatively regulating inflammation and angiogenesis, thereby contributing to the maintenance of vascular quiescence (24–27). KLF2 inhibits cytokine-mediated induction of pro-inflammatory targets such as vascular cell adhesion molecule-1 (VCAM-1) and E-selectin (24, 25). In addition to anti-inflammatory action, KLF2 also down-regulates expression of vascular endothelial growth factor (VEGF) receptor 2 (VEGFR2), leading to the inhibition of VEGF-induced angiogenesis and hyperpermeability (26, 27). Similarly, Ang1 functions as an anti-inflammatory and anti-permeability factor (6, 29). Ang1 inhibits VEGF-stimulated leukocyte adhesion to endothelium by reducing expression of cell adhesion molecules such as VCAM-1 and E-selectin (30). Furthermore, Ang1 counteracts VEGF-induced hyperpermeability *in vitro* and *in vivo* (29, 31–33). Our previous data that Ang1 induced KLF2 expression (10) and the common roles by Ang1 and KLF2 for vascular quiescence prompted us to test our hypothesis that Ang1/Tie2 signal may maintain the vascular quiescence through KLF2 induction and to investigate how KLF2 is induced by Ang1/Tie2 signaling.

In this study, we found that Ang1/Tie2 signal stimulates transcriptional activity of MEF2 through a phosphoinositide 3-kinase (PI3K)/AKT pathway to induce KLF2 expression. Moreover, we revealed that Ang1-induced signaling functionally competes with VEGF-induced inflammatory responses.

EXPERIMENTAL PROCEDURES

Reagents, Antibodies, siRNAs, and Recombinant Protein—Ang1 and cartilage oligomeric matrix protein (COMP)-Ang1 were prepared as described before (34). VEGF was purchased from R&D Systems. Wortmannin and AKT inhibitor IV were obtained from Calbiochem. We generated anti-KLF2 monoclonal antibody against amino acids 2–34 of human KLF2. Anti-green fluorescent protein (GFP) antibody was prepared as described before (35). Other antibodies were purchased as follows: anti-tubulin, anti-ERK5, anti-FLAG (M2), and anti-β-actin from Sigma-Aldrich; anti-MEF2 from Santa Cruz Biotechnology; anti-phospho-AKT, anti-AKT, anti-phospho-ERK1/2, and anti-ERK1/2 from Cell Signaling Technology; horseradish peroxidase-coupled sheep anti-mouse and anti-rabbit IgG from GE Healthcare Life Sciences; and Alexa Fluor 488-labeled secondary antibody from Molecular Probes. Stealth siRNAs targeting the genes indicated below were purchased from Invitrogen: human *KLF2* (HSS145585, HSS145587), human *ERK5* (HSS140815), human *AKT1* (validated stealth RNA interference: 12935-001), human *AKT2* (validated stealth RNA interference: 12937-40), human *MEF2A* (HSS106435, HSS106436), human *MEF2C* (HSS106438, HSS106439), and human *MEF2D* (HSS106441, HSS106442). Glutathione *S*-transferase (GST) fusion protein containing transactivating domain of MEF2C (GST-MEF2C) was prepared as described before (36).

Plasmids and Adenoviruses—A luciferase reporter plasmid containing the proximal 221-bp region of KLF2 promoter (KLF2wt-Luc) was kindly provided by M. K. Jain (Case Western Reserve University). The MEF2-binding site of the KLF2wt-Luc plasmid was mutated using the QuikChange site-directed mutagenesis kit (Stratagene) using the KLF2wt-Luc vector as a template. Expression plasmids encoding MEF2C and constitutive active mutants of AKT (pCEFL-myrAKT) and PI3K-γ (pcDNA3-PI3Kγ-CAAX) and a luciferase reporter plasmid containing a single MEF2-binding site (pGL3-MEF2) have already been described (36–38). A cDNA encoding full-length MEF2C amplified by PCR using pCEFL-GST-MEF2C as a template was inserted into p3xFLAG CMV10 vector (Sigma-Aldrich) or cloned into pCMV-DBD vector (Stratagene) to construct the plasmid expressing a Gal4 DNA-binding domain (DBD)-MEF2C fusion protein (Gal4/MEF2C). Plasmids encoding Gal4/MEF2C mutant proteins (Thr-293, Thr-300, Ser-387 (phosphorylation sites by ERK5 and p38), and Thr-404 (potential phosphorylation site by AKT) were replaced with Ala, and 6 Lys residues (Lys-116, Lys-119, Lys-234, Lys-239, Lys-252, Lys-264; acetylation sites by p300) replaced with Arg were generated using the QuikChange site-directed mutagenesis kit. An expression vector encoding FLAG-tagged HDAC5 was generously obtained from C. Grozinger (Harvard University). Other vectors are purchased as follows: pRL-SV40 and pRL-TK from Promega Corp.; pEGFP-C1 from Clontech; and pFR from Stratagene. Recombinant adenovirus vectors encoding GFP and constitutively active form of AKT were kindly provided by H. Kurose (Kyushu University) and Y. Fujio (Osaka University), respectively.

Cell Culture, Transfection, siRNA-mediated Protein Knockdown, and Adenovirus Infection—Human umbilical vein endothelial cells (HUVECs) were cultured as described previously (10) and used for experiments before passage 7. HUVECs were placed on collagen-coated plates at a density of 2,000 cells/cm^2 and 40,000 cells/cm^2 and cultured overnight to obtain sparse and confluent cell cultures, respectively. U937 cells, a human monocyte-like cell line, were cultured in RPMI 1640 (Invitrogen) supplemented with 10% fetal bovine serum, 50 units/ml penicillin, and 50 μg/ml streptomycin. HUVECs were transfected using Lipofectamine 2000 reagent (Invitrogen) and Lipofectamine Plus reagent (Invitrogen) according to the manufac-

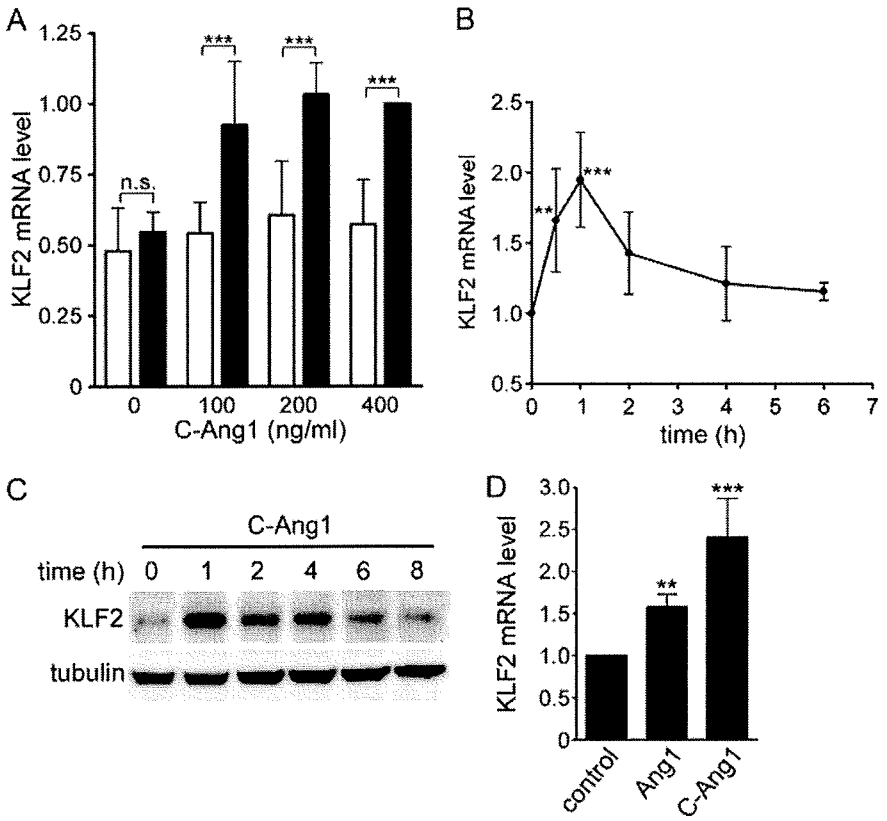

FIGURE 1. **Ang1 induces KLF2 expression in confluent HUVECs.** *A*, sparse (*open bars*) and confluent (*closed bars*) HUVECs were starved in medium 199 containing 1% BSA for 6 h and stimulated with COMP-Ang1 (*C-Ang1*) at the concentrations indicated at the *bottom* (ng/ml) for 1 h. After the stimulation, total RNA was extracted and subjected to real-time RT-PCR analysis to determine the expression level of KLF2 mRNA as described under "Experimental Procedures." Bar graphs show relative mRNA levels of *KLF2* normalized to that of *GAPDH*. KLF2 mRNA levels are expressed relative to that in confluent cells stimulated with 400 ng/ml COMP-Ang1. Data are shown as means ± S.D. of six independent experiments. *B*, confluent HUVECs starved for 6 h were stimulated with 400 ng/ml COMP-Ang1 for the periods indicated at the *bottom* (h) (COMP-Ang1 was used at the concentration of 400 ng/ml throughout the following experiments). KLF2 mRNA levels were analyzed by real-time RT-PCR as described in *A*. Values are expressed relative to that in the unstimulated cells and shown as means ± S.D. of five independent experiments. *C*, confluent HUVECs were starved in HuMedia EB2 medium containing 0.5% fetal calf serum for 12 h and stimulated with COMP-Ang1 for the periods indicated at the *top* (h). Cell lysates were subjected to Western blot analysis with anti-KLF2 (*top panel*) and anti-tubulin (*bottom panel*) antibodies. *D*, confluent HUVECs were stimulated with vehicle (*control*), 600 ng/ml Ang1 (*Ang1*), and COMP-Ang1 (*C-Ang1*) for 1 h. KLF2 mRNA levels were determined as described in *A*. Values are expressed relative to that in the control cells and shown as means ± S.D. of six independent experiments. Significant differences between two groups (*A*) or from the control (*B* and *D*) are indicated as **, $p < 0.01$ or ***, $p < 0.001$. *n.s.* indicates no significance between two groups.

turer's instructions. For siRNA-mediated gene silencing, HUVECs were transfected with siRNA duplexes using Lipofectamine RNAiMAX reagent (Invitrogen) and used for the experiments 48–72 h after transfection. HUVECs were infected with adenovirus vectors at the appropriate multiplicity of infection. Forty-eight h after infection, the cells were used for experiments.

Real-time Reverse Transcription-PCR—Sparse and confluent HUVECs placed on collagen-coated plates were starved in medium 199 containing 1% BSA for 6 h and stimulated with COMP-Ang1 as described in the figure legends. The cells were stimulated in the presence of 30 μM wortmannin or 8 μM AKT inhibitor IV. To examine the effect of COMP-Ang1 on VEGF-induced VCAM-1 expression, HUVECs starved in medium 199 containing 0.5% BSA for 5 h were prestimulated with or without COMP-Ang1 for 1 h and subsequently challenged with VEGF for 3 h. After the stimulation, total RNA was purified using TRIzol (Invitrogen). Quantitative real-time reverse transcription (RT)-PCR was carried out using QuantiFast SYBR Green RT-PCR kit (Qiagen) as described before (10). For each reaction, 100 ng of total RNA was transcribed for 10 min at 50 °C followed by a denaturing step at 95 °C for 5 min and 40 cycles of 10 s at 95 °C and 30 s at 60 °C. Fluorescence data were collected and analyzed using Mastercycler ep realplex (Eppendorf). The primers used for amplification were as follows: for human *KLF2*, 5′-CTACACCAAGAGTTCGCATCTG-3′ and 5′-CCGTGTGCTTTCGGTAGTG-3′; for human *VCAM1*, 5′-CAAATCCTTGATACTGCTCATC-3′ and 5′-TTGACTTCTTGCTCACAGC-3′; for *glyceraldehyde-3-phosphate dehydrogenase* (*GAPDH*), 5′-ATGGGGAAGGTGAAGGTCG-3′ and 5′-GGGGTCATTGATGGCAACAATA-3′. For normalization, expression of human *GAPDH* was determined in parallel as an endogenous control.

Detection of KLF2 Protein Expression—To examine the KLF2 protein expression induced by COMP-Ang1, confluent HUVECs plated on a collagen-coated dish were starved in Humedia-EB2 medium (Kurabo) containing 0.5% fetal calf serum for 12 h and stimulated with 400 ng/ml COMP-Ang1 for the periods as indicated in the figure legends. After the stimulation, the cells were washed once with ice-cold phosphate-buffered saline, harvested by scraping, and pelleted by centrifugation at 4,000 × *g* for 10 min at 4 °C. The cell pellets were then lysed at 4 °C in radioimmune precipitation buffer containing 50 mM Tris-HCl at pH 7.5, 150 mM NaCl, 1% Triton X-100, 0.5% sodium deoxycholate, 0.1% sodium dodecyl sulfate, and 1× protease inhibitor mixture. The cell lysates were subjected to SDS-PAGE and Western blot analysis as described previously (39).

Detection of ERK5, AKT, and ERK1/2 Activities—Confluent and sparse HUVECs plated on collagen-coated dish were starved in medium 199 containing 1% BSA for 6 h and stimulated with 400 ng/ml COMP-Ang1 for 15 min. The cells were then lysed at 4 °C in lysis buffer containing 25 mM HEPES at pH 7.5, 0.3 M NaCl, 1.5 mM $MgCl_2$, 0.2 mM EDTA, 0.5 mM dithiothreitol, 20 mM β-glycerophosphate, 1 mM sodium vanadate, 1% Triton X-100, and 1× protease inhibitor mixture. To meas-

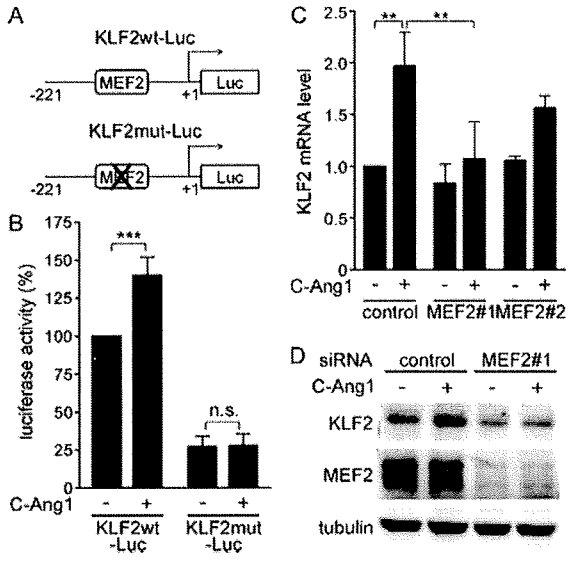

FIGURE 2. **MEF2 is responsible for Ang1-induced KLF2 expression.** *A*, structures of KLF2wt-Luc and KLF2mut-Luc reporter constructs are shown. *B*, confluent HUVECs were transfected with either KLF2wt-Luc (*left*) or KLF2mut-Luc (*right*) reporter construct together with pRL-SV40 vector. After transfection, the cells were stimulated without (−) or with (+) COMP-Ang1 (*C-Ang1*) in 1% BSA-containing medium 199 for 24 h. The medium was replaced with the freshly prepared same medium every 6 h. After the stimulation, the cells were collected, and the lysates were assayed for firefly and *Renilla* luciferase activities as described under "Experimental Procedures." The data represent firefly luciferase activity normalized by the *Renilla* luciferase activity present in each cellular lysate. Values are expressed as a percentage relative to that observed in the KLF2wt-Luc transfected cells treated with vehicle and shown as mean ± S.D. of three independent experiments. *C*, confluent HUVECs transfected with control siRNA (*control*) or with two independent MEF2 siRNA mixtures (*MEF2#1* and *MEF2#2*: each mixture contains siRNAs targeting MEF2A, MEF2C, and MEF2D) were stimulated as described in the legend for Fig. 1 (*panel D*). KLF2 mRNA levels were determined as described in the legend for Fig. 1 (*panel A*). Values are expressed relative to that in the control siRNA-transfected cells treated with vehicle and shown as means ± S.D. of three independent experiments. *D*, confluent HUVECs transfected with control siRNA or with MEF2 siRNA mixture (*MEF2#1*) were starved and stimulated with vehicle (−) or COMP-Ang1 (+) as described in the legend for Fig. 1 (*panel C*). Cell lysates were subjected to Western blot analysis with anti-KLF2 (*top panel*), anti-MEF2 (middle panel), and anti-tubulin (*bottom panel*) antibodies. In B and C, significant differences between two groups are indicated as **, $p < 0.01$, or ***, $p < 0.001$. *n.s.* indicates no significance between two groups.

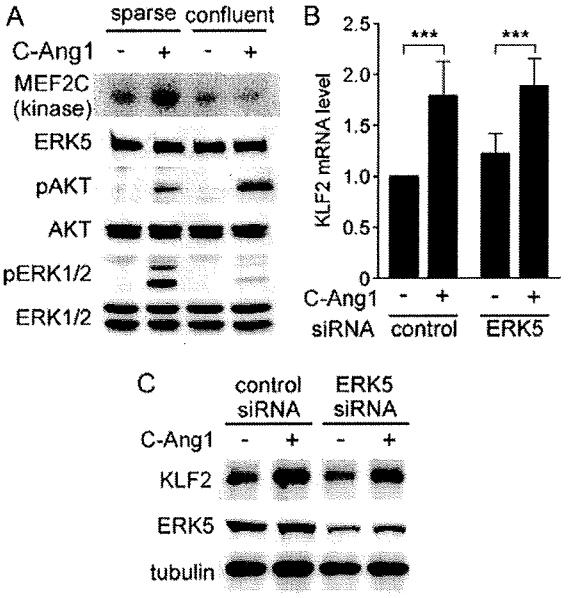

FIGURE 3. **Ang1-induced KLF2 expression does not require ERK5.** *A*, sparse (*left*) and confluent (*right*) HUVECs were starved in medium 199 containing 1% BSA for 6 h and stimulated with vehicle (−) or COMP-Ang1 (*C-Ang1*) (+) for 15 min. To measure the ERK5 activity, *in vitro* kinase assay was performed using anti-ERK5 immunoprecipitates from the corresponding cell lysates as described under "Experimental Procedures." ^{32}P-labeled substrates are shown at the *top* (*MEF2C (kinase)*). In parallel, cell lysates were subjected to Western blot analysis with anti-ERK5 (*ERK5*), anti-phosphoAKT (*pAKT*), anti-AKT (*AKT*), anti-phosphoERK1/2 (*pERK1/2*), and anti-ERK1/2 (*ERK1/2*) antibodies. *B*, confluent HUVECs transfected with control siRNA (*left*) or ERK5 siRNA (*right*) were starved and stimulated with vehicle (−) or COMP-Ang1 (+) as described in the legend for Fig. 1 (*panel D*). KLF2 mRNA levels were determined and expressed as described in the legend for Fig. 2 (*panel C*). Values are shown as means ± S.D. of five independent experiments. Significant differences between two groups are indicated as ***, $p < 0.001$. *C*, confluent HUVECs transfected with control or ERK5 siRNA were starved and stimulated as described in the legend for Fig. 1 (*panel C*). Cell lysates were subjected to Western blot analysis with anti-KLF2 (*top panel*), anti-ERK5 (*middle panel*), and anti-tubulin (*bottom panel*) antibodies.

ure the ERK5 activity, *in vitro* kinase assay was performed as described previously (40). Briefly, endogenous ERK5 was immunoprecipitated from aliquots of cell lysate with anti-ERK5 antibody at 4 °C for 3 h, and the immunocomplexes were recovered with protein G-Sepharose beads (GE Healthcare Life Sciences). Beads were washed three times with phosphate-buffered saline containing 1% Nonidet P-40 and 2 mM sodium vanadate, once with washing buffer containing 100 mM Tris at pH 7.5 and 0.5 M LiCl and once with kinase reaction buffer containing 12.5 mM MOPS at pH 7.5, 12.5 mM β-glycerophosphate, 7.5 mM $MgCl_2$, 0.5 mM EGTA, 0.5 mM sodium vanadate, and 0.5 mM sodium fluoride. Samples were then resuspended in 15 μl of kinase reaction buffer containing 3 μg of GST-MEF2C, 1 μCi of [γ-^{32}P]ATP, and 20 μM cold ATP and incubated at 37 °C for 90 min. ^{32}P-labeled substrates were separated by SDS-PAGE and detected by autoradiography. To evaluate the phosphorylation of AKT and ERK1/2, aliquots of cell lysate were subjected to Western blot analysis with anti-phospho-AKT and anti-phospho-ERK1/2 antibodies, respectively. The total contents of ERK5, AKT, and ERK1/2 in each cell lysate were also assayed in a parallel run using corresponding antibodies.

Luciferase Reporter Assay—Luciferase reporter assay was carried out as described before (36, 40). Confluent HUVECs plated on a collagen-coated 12-well plate were transfected with different expression vectors, together with reporter plasmids as described in the figure legends. The total amount of plasmid DNA was adjusted with empty vector. To examine the effect of COMP-Ang1, the cells were starved and stimulated as described in the figure legends. The cells were lysed using passive lysis buffer (Promega), and luciferase activities in cell extract were determined using a Dual-Luciferase assay system (Promega).

Detection of Subcellular Localization of FLAG-tagged HDAC5—Confluent HUVECs plated on a collagen-coated glass base dish were transfected with the plasmid encoding FLAG-tagged histone deacetylase (HDAC) 5. Twenty-four h after the transfection, the cells were starved in medium 199 containing 0.5% BSA for 6 h and subsequently stimulated with vehicle, COMP-Ang1, or VEGF for 3 h. After the stimulation, the cells were fixed and stained with anti-FLAG antibody as

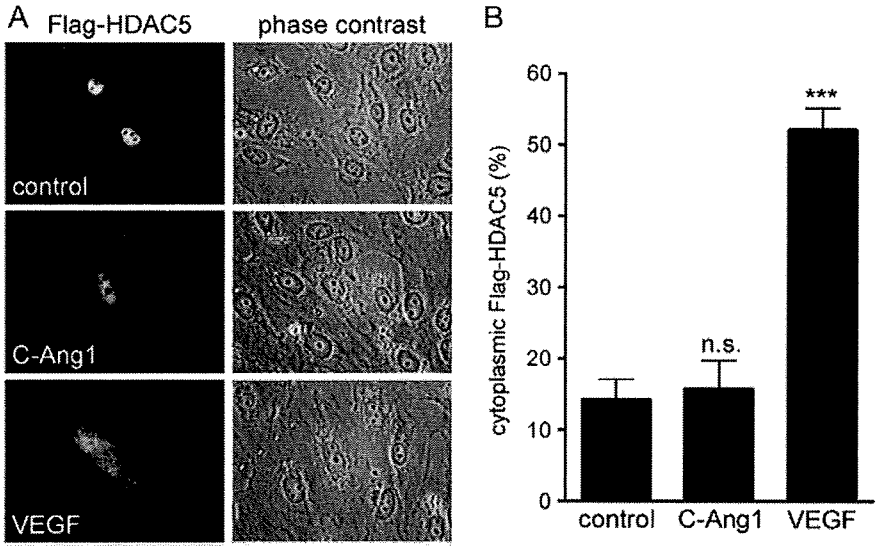

FIGURE 4. **Ang1 does not induce nuclear export of HDAC5.** *A*, confluent HUVECs plated on a collagen-coated glass base dish were transfected with the plasmid encoding FLAG-tagged HDAC5. After 24 h, the cells were starved in medium 199 containing 0.5% BSA for 6 h and stimulated with vehicle (*control*: *upper panel*), COMP-Ang1 (*C-Ang1*: *middle panel*), or 50 ng/ml VEGF (*bottom panel*) for 3 h. After the stimulation, the cells were fixed, immunostained with anti-FLAG antibody, and visualized with Alexa Fluor 488-conjugated secondary antibody. Alexa Fluor 488 and phase contrast images are shown at the *left* and *right columns*, respectively. *B*, nuclear export of HDAC5 by vehicle (*control*), COMP-Ang1 (*C-Ang1*), and VEGF observed in *A* was quantified. The number of cells expressing FLAG-tagged HDAC5 in the cytoplasm was counted and expressed as a percentage relative to the total number of cells expressing FLAG-tagged HDAC5. At least 100 cells were scored for each treatment. Values are expressed as means ± S.D. of three independent experiments. Significant difference from the control is indicated as ***, $p < 0.001$. *n.s.* indicates no significant difference from the control.

described before (10). Protein reacting with antibody was visualized with Alexa Fluor 488-conjugated secondary antibody. Alexa Fluor 488 and phase contrast images were recorded with an Olympus IX-81 inverted fluorescence microscope. The number of cells expressing FLAG-tagged HDAC5 in the cytoplasm among FLAG-tagged HADC5-expressing cells was counted. Nuclear export of HDAC5 was determined by the HDAC5 in the cytoplasm instead of the nucleus. At least 100 cells were scored for each experiment.

Monocyte Adhesion Assay—HUVECs transfected with control or KLF2 siRNA were placed on collagen-coated 24-well plates at the density of 40,000 cells/cm^2, cultured overnight, and starved in medium 199 containing 1% BSA for 2 h. The cells were prestimulated with 400 ng/ml COMP-Ang1 for 1 h and challenged with vehicle or 50 ng/ml VEGF in the presence or absence of COMP-Ang1 for 4 h. U937 cells labeled with green fluorescent dye PKH67 (Sigma-Aldrich) were added to the confluent HUVEC monolayers (8×10^5 cells/well) and incubated in RPMI 1640 containing 1% fetal bovine serum for 90 min. The cells were then washed three times with prewarmed Hank's buffered salt solution (Invitrogen) and fixed with 2% formaldehyde. Phase contrast and PKH67 fluorescent images were recorded with an Olympus IX-81 inverted fluorescence microscope. The adherent U937 cells were quantified by measuring fluorescent intensity at five randomly selected fields in each well using MetaMorph 6.1 software (Molecular Devices Corp.).

Statistical Analysis—The values are expressed as means ± S.D. Statistical significance was determined using one-way analysis of variance, two-way analysis of variance, or unpaired *t* test. *p* values < 0.05 were considered statistically significant.

RESULTS

Ang1 Induces KLF2 Expression in Confluent but Not Sparse Cultures of HUVECs—To first examine the KLF2 expression downstream of *trans*-associated Tie2 at cell-cell contacts and cell-substratum contact-anchored Tie2 in response to Ang1, HUVECs were stimulated with COMP-Ang1, a potent Ang1 variant, under either confluent or sparse culture condition. COMP-Ang1 concentration-dependently induced KLF2 mRNA expression in confluent HUVECs but not in the sparse cells (Fig. 1*A*). Consistently, KLF2 protein expression was up-regulated upon stimulation with COMP-Ang1 (Fig. 1*C*). KLF2 mRNA and protein expression by COMP-Ang1 peaked at 1 h after the stimulation and then declined to the basal level by 6 h (Fig. 1, *B* and *C*). KLF2 mRNA level was increased in response to native Ang1 as well as COMP-Ang1 (Fig. 1*D*). Taken together with the previously reported evidence that Ang1 induces *trans*-association of Tie2 in the presence of cell-cell contacts (10, 11), these results suggest that *trans*-associated Tie2 at cell-cell contacts is capable of inducing KLF2 expression.

Ang1 Induces KLF2 Expression through MEF2—Next, we sought to delineate the signaling pathway responsible for Ang1-induced KLF2 expression. It has been reported that laminar shear stress and statins activate the KLF2 promoter via a single MEF2-binding site located at −120/−111 bp upstream from the transcriptional initiation site (19, 41, 42). Thus, we investigated the role of MEF2 in Ang1-induced KLF2 expression. HUVECs were transfected with either luciferase reporter plasmid in which the reporter is driven by the proximal 221-bp region (−221 bp upstream from the initiation site) of KLF2 promoter (KLF2wt-Luc) or by its MEF2-binding site-mutated promoter (KLF2mut-Luc) (Fig. 2*A*). COMP-Ang1 significantly induced KLF2 promoter-regulated reporter activity, whereas it failed to induce reporter activation when KLF2 promoter lacked MEF2-binding site (Fig. 2*B*), suggesting the indispensable role of MEF2 in Ang1-induced KLF2 expression. To further confirm the requirement of MEF2 for Ang1-induced KLF2 expression, we employed an siRNA technique to down-regulate MEF2 family proteins including MEF2A, MEF2C, and MEF2D. Depletion of these MEF2 proteins inhibited COMP-Ang1-induced both KLF2 mRNA expression and KLF2 protein expression (Fig. 2, *C* and *D* and supplemental Fig. S1). These findings

indicate that KLF2 expression induced by Ang1 depends upon MEF2.

Ang1-induced KLF2 Expression Is Not Mediated by the Signaling Pathways Involving ERK5 and HDAC5—ERK5 stimulates transcriptional activity of MEF2 factors by phosphorylating their transactivating domains (36, 43, 44). Previous reports indicate that KLF2 expression is severely impaired in ERK5-null mouse embryo (45) and that laminar shear stress stimulates ERK5 activity to induce MEF2-dependent KLF2 expression (19). Therefore, we examined whether Ang1 stimulates ERK5 activity under either confluent or sparse conditions to investigate the involvement of ERK5 in KLF2 induction by Ang1. COMP-Ang1 preferentially activated ERK5 as well as ERK1/2 in sparse HUVECs (Fig. 3*A*). However, stimulation of confluent cells with COMP-Ang1 did not enhance ERK5 kinase activity, although AKT was potently activated under this condition (Fig. 3*A*). These results suggest that Ang1 induces KLF2 expression independently of ERK5. Consistently, depletion of ERK5 by siRNAs did not affect COMP-Ang1-induced KLF2 mRNA and protein expression (Fig. 3, *B* and *C*).

Class II HDACs, consisting of HDAC4, HDAC5, HDAC7, and HDAC9, interact with MEF2 and repress the expression of MEF2 target genes (46). Phosphorylation of class II HDACs by calcium/calmodulin-dependent protein kinase and protein kinase D results in their nuclear exclusion, leading to the enhancement of MEF2 transcriptional activity (46–48). Therefore, we examined whether Ang1 induces nuclear export of class II HDACs to enhance MEF2 activity. COMP-Ang1 did not induce nuclear export of FLAG-tagged HDAC5, although VEGF did (Fig. 4), suggesting that Ang1-induced KLF2 expression does not depend upon the inhibition of class II HDACs.

A PI3K/AKT Pathway Is Responsible for Ang1-induced KLF2 Expression—Ang1 is able to induce KLF2 expression only under confluent condition as described above (Fig. 1*A*). Under this condition, an AKT pathway is preferentially activated by Ang1 (Fig. 3*A*). These evidences prompted us to investigate whether the AKT pathway is responsible for KLF2 induction by Ang1. COMP-Ang1-induced KLF2 expression was completely blocked by wortmannin and AKT inhibitor IV, inhibitors for PI3K and AKT, respectively (Fig. 5, *A* and *B*). Furthermore, we examined the involvement of AKT in Ang1-meditaed KLF2 expression by depleting AKT using siRNAs for AKT. Depletion of AKT prevented both COMP-Ang1-induced KLF2 mRNA expression and COMP-Ang1-induced KLF2 protein expression (Fig. 5, *C* and *D*). These results indicate that a PI3K/AKT pathway is indispensable for Ang1-induced KLF2 expression.

A PI3K/AKT Pathway Stimulates Transcriptional Activity of MEF2—To clarify whether a PI3K/AKT pathway stimulates MEF2-dependent transcription, HUVECs were transfected with a plasmid expressing luciferase reporter gene under the control of a single MEF2 site (MEF2-Luc) together with the plasmid encoding constitutive active AKT (AKT-CA) or PI3K (PI3K-CA). The reporter gene activity was only slightly stimulated by AKT-CA or PI3K-CA (Fig. 6*A*). However, coexpression of MEF2C significantly enhanced AKT-CA- or PI3K-CA-induced reporter gene expression (Fig. 6*A*). To further investigate whether MEF2-dependent transcription stimulated by

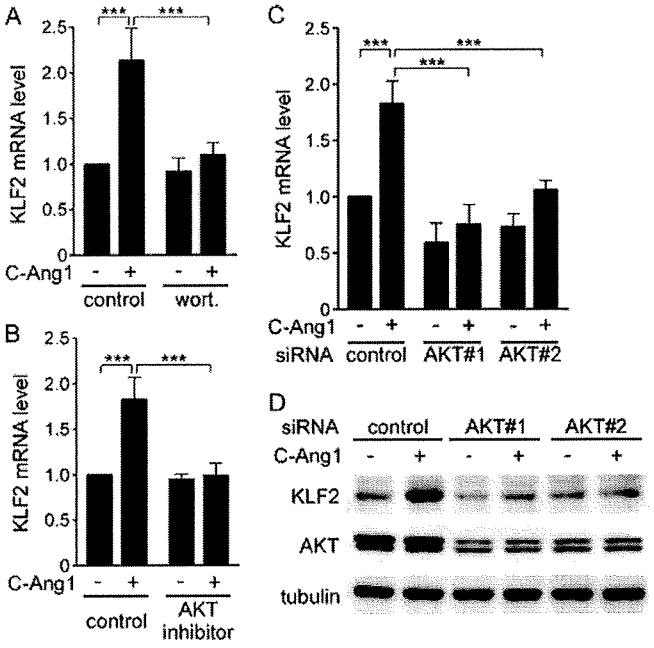

FIGURE 5. **A PI3K/AKT pathway is involved in Ang1-induced KLF2 expression.** *A*, confluent HUVECs starved for 6 h were pretreated with vehicle (*control*) or 30 nM wortmannin (*wort.*) for 30 min and subsequently stimulated with vehicle (−) or COMP-Ang1 (*C-Ang1*) (+) for 1 h. KLF2 mRNA levels were determined as described in the legend for Fig. 1 (*panel A*). Values are expressed relative to that in the wortmannin-untreated cells stimulated with vehicle and shown as means ± S.D. of five independent experiments. *B*, confluent HUVECs starved for 6 h were pretreated with vehicle (*control*) or 8 μM AKT inhibitor for 10 min and subsequently stimulated with vehicle (−) or COMP-Ang1 (+) for 1 h. KLF2 mRNA levels were determined and expressed as described in *A*. Data are shown as means ± S.D. of four independent experiments. *C*, confluent HUVECs transfected with control siRNA (*control*) or with two independent AKT siRNA mixtures (*AKT#1* and *AKT#2*: each mixture contains siRNAs targeting AKT1 and AKT2) were starved and stimulated as described in the legend for Fig. 1 (*panel D*). KLF2 mRNA levels were determined and expressed as described in the legend for Fig. 2 (*panel C*). Values are shown as means ± S.D. of four independent experiments. *D*, confluent HUVECs transfected with control siRNA or with two independent AKT siRNA mixtures (*AKT#1* and *AKT#2*) were starved and stimulated as described in the legend for Fig. 1 (*panel C*). Cell lysates were subjected to Western blot analysis with anti-KLF2 (*top panel*), anti-AKT (*middle panel*), and anti-tubulin (*bottom panel*) antibodies. In *A–C*, significant differences between two groups are indicated as ***, $p < 0.001$.

PI3K-CA and AKT-CA is ascribed to the enhanced transcriptional activity, we fused full-length MEF2C with DNA-binding domain of yeast Gal4 protein (Gal4/MEF2C) and tested the direct effect of AKT and PI3K on transcriptional activity of Gal4/MEF2C. AKT-CA and PI3K-CA potently stimulated the transcriptional activity of Gal4/MEF2C but not that of Gal4 (Fig. 6*B*). In addition, stimulation with COMP-Ang1 evoked Gal4/MEF2C-dependent reporter gene expression (Fig. 6*C*). Collectively, these findings indicate that Ang1/Tie2 signal stimulates the transcriptional activity of MEF2 through a PI3K/AKT pathway.

A PI3K/AKT/MEF2 Signaling Axis Stimulates the KLF2 Promoter—We further investigated the functional role of a PI3K/AKT/MEF2 pathway in Ang1-induced KLF2 expression. When HUVECs were transfected with the KLF2wt-Luc reporter gene along with the plasmid encoding GFP, AKT-CA, or PI3K-CA, AKT-CA and PI3K-CA induced more luciferase expression than GFP (Fig. 6*D*). The stimulatory effects of

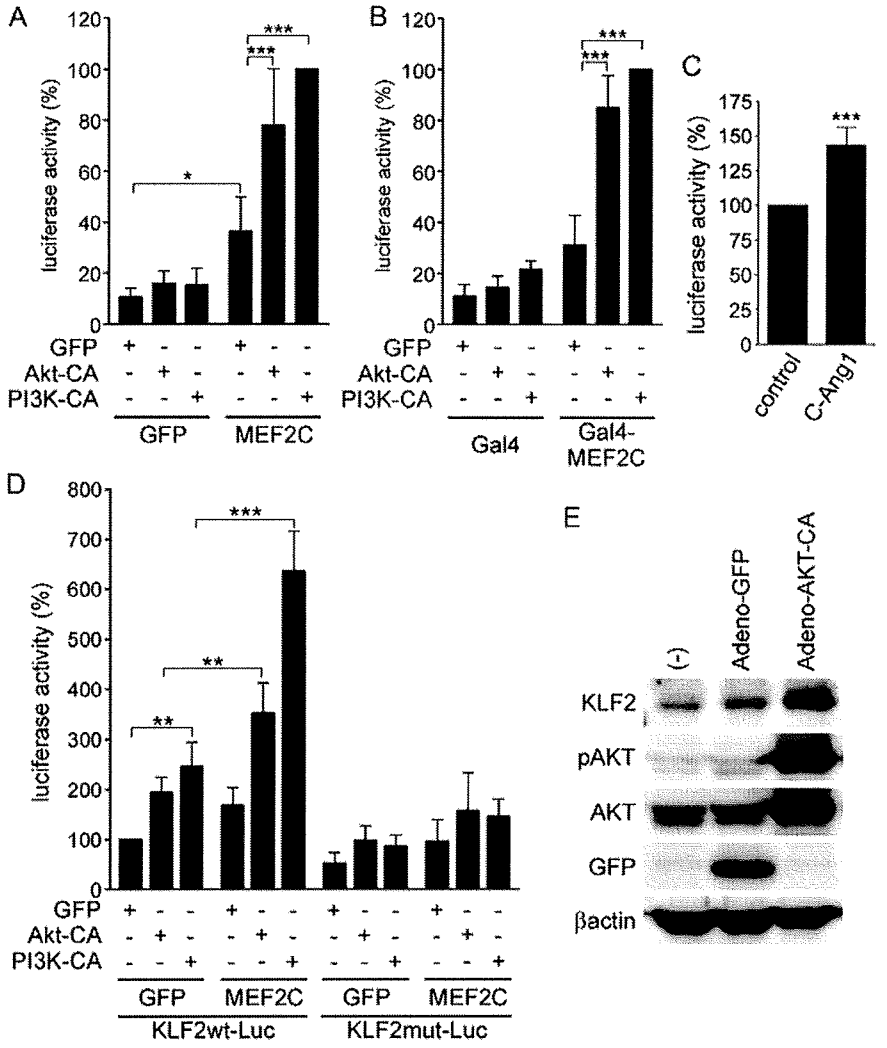

FIGURE 6. **A PI3K/AKT pathway stimulates transcriptional activity of MEF2, leading to KLF2 expression.** *A*, confluent HUVECs were cotransfected with pGL3-MEF2 and pRL-TK vectors, together with the plasmid encoding either GFP or MEF2C as indicated at the *bottom*. The expression vector for GFP, AKT-CA, or PI3K-CA was also included in the transfection mixture as shown at the *left*. The cells were lysed 24 h after the transfection. Luciferase activities were assayed and presented as described in the legend for Fig. 2 (*panel B*). Data are expressed as a percentage relative to that observed in the cells expressing both PI3K-CA and MEF2C and shown as mean ± S.D. of four independent experiments. *B*, confluent HUVECs were cotransfected with pFR and pRL-TK vectors, along with the plasmid expressing either Gal4 (*left*) or Gal4-MEF2C (*right*) as indicated at the *bottom*. The expression vector for GFP, AKT-CA, or PI3K-CA was also included in the transfection mixture as shown at the *left*. After 24 h of incubation, luciferase activities were assayed and represented as described in the legend for Fig. 2 (*panel B*). Data are expressed as a percentage relative to that observed in the cells expressing both Gal4-MEF2C and PI3K-CA and shown as mean ± S.D. of three independent experiments. *C*, confluent HUVECs transfected with the plasmid encoding Gal4-MEF2C together with pGal4-Luc and pRL-SV40 reporter plasmids were starved and stimulated as described in the legend for Fig. 2 (*panel B*). Luciferase activities were assayed and presented as described in the legend for Fig. 2 (*panel B*). Data are expressed as a percentage relative to that observed in the control cells and shown as mean ± S.D. of four independent experiments. *D*, confluent HUVECs were cotransfected with pRL-TK vector, along with either KLF2wt-Luc or KLF2mut-Luc reporter gene, and also with the expression vector for either GFP or MEF2C as indicated at the *bottom*. The plasmid encoding GFP, AKT-CA, or PI3K-CA was also included in the transfection mixture as shown at the *left*. Twenty-four h after the transfection, luciferase activities were assayed and presented as described in the legend for Fig. 2 (*panel B*). Data are expressed as a percentage relative to that in the cells transfected with KLF2wt-Luc along with the vector encoding GFP and shown as mean ± S.D. of four independent experiments. *E*, confluent HUVECs were infected without (−) or with adenoviruses encoding either GFP or AKT-CA as indicated at the *top*. Forty-eight h after infection, the cells were collected, and the lysates were subjected to Western blot analysis with anti-KLF2 (*KLF2*), anti-phosphoAKT (*pAKT*), anti-AKT (*AKT*), anti-GFP (*GFP*), and anti-β-actin (*βactin*) antibodies. Significant differences between two groups (*A*, *B*, and *D*) or from the control (*C*) are indicated as *, $p < 0.05$, **, $p < 0.01$, or ***, $p < 0.001$.

AKT-CA and PI3K-CA on the reporter gene activity were significantly augmented by coexpression of MEF2C (Fig. 6*D*). AKT-CA and PI3K-CA did not stimulate the luciferase expression driven by the mutant promoter that lacks the MEF2-binding site (the KLF2mut-Luc), even in the presence of MEF2C (Fig. 6*D*). In addition, adenovirus-mediated overexpression of AKT-CA potently induced both mRNA and protein expression of KLF2 in HUVECs (Fig. 6*E* and supplemental Fig. S2). Collectively, these results suggest that Ang1/Tie2 signal induces KLF2 expression through a PI3K/AKT/MEF2 signaling axis.

How does a PI3K/AKT signaling enhance transcriptional activity of MEF2? MEF2 activity is known to be regulated by its posttranslational modification such as phosphorylation and acetylation (49). We examined the effect of a PI3K/AKT pathway on posttranslational modification of MEF2C. We constructed the plasmids encoding Gal4/MEF2C mutants: 1) Gal4/MEF2C-ERK5/p38mut in which potential phosphorylation sites of MEF2C by p38 and ERK5 mitogen-activated protein (MAP) kinases (Thr-293, Thr-300, and Ser-387 corresponding to those in human MEF2C) were replaced by Ala (43, 50) and 2) Gal4/MEF2C-AKT mutant in which consensus phosphorylation site of MEF2C by AKT (Thr-404 corresponding that in human MEF2C) was mutated to Ala; and 3) Gal4/MEF2C-6KR in which the 6 Lys residues in MEF2C acetylated by p300 (Lys-116, Lys-119, Lys-234, Lys-239, Lys-252, and Lys-264 corresponding to those in human MEF2C) were replaced by Arg (51). Using these plasmids, MEF2-dependent transcription was directly tested in the cells expressing PI3K-CA. Expression of PI3K-CA could stimulate transcriptional activity mediated by mutant MEF2C to a similar extent to wild type MEF2C (supplemental Fig. S3). These results suggest that the posttranslational modification by ERK5, p38, AKT, and p300 is not required for PI3K/AKT pathway-stimulated MEF2 transcriptional activity.

Angl Inhibits VEGF-induced Inflammatory Responses through KLF2—We finally addressed the significance of Angl/Tie2-dependent KLF2 expression in the cells. KLF2 has potent

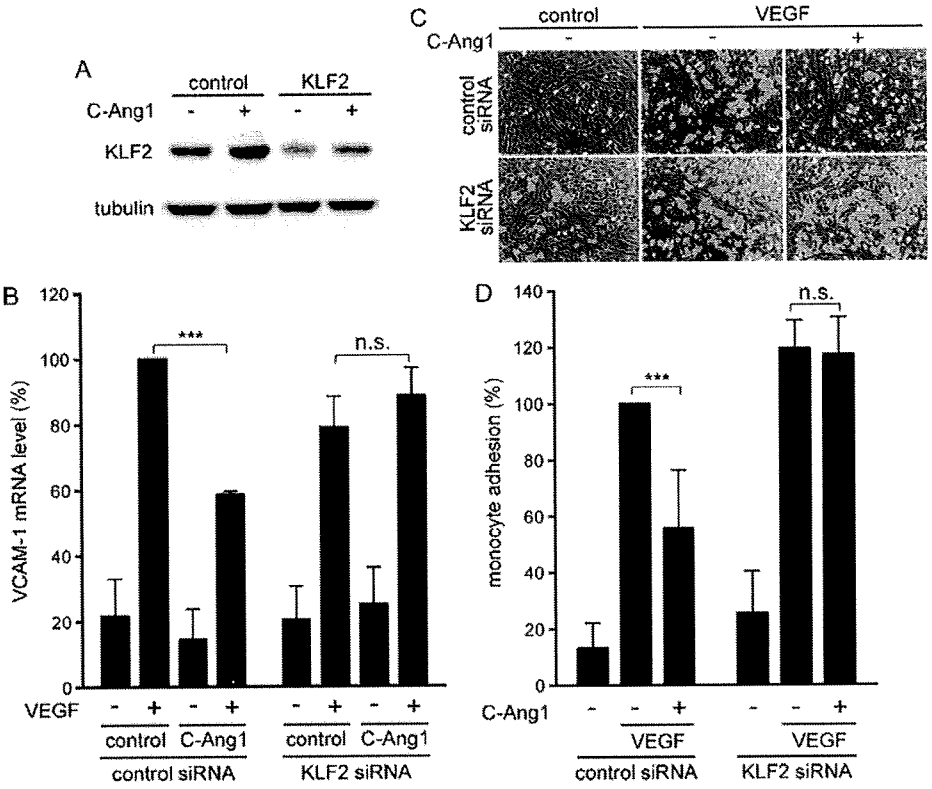

FIGURE 7. **KLF2 is responsible for the inhibitory effect of Ang1 on VEGF-induced inflammation.** *A*, confluent HUVECs transfected with control or KLF2 siRNA were starved and stimulated as described in the legend for Fig. 1 (*panel C*). Cell lysates were subjected to Western blot analysis with anti-KLF2 (*top panel*) and anti-tubulin (*bottom panel*) antibodies. *B*, confluent HUVECs transfected with control or KLF2 siRNA were starved in medium 199 containing 0.5% BSA for 6 h. The cells prestimulated with or without COMP-Ang1 (*C-Ang1*) for 1 h were challenged with vehicle (−) or 50 ng/ml VEGF (+) for 3 h. VCAM-1 mRNA levels were analyzed by real-time RT-PCR as described in the legend for Fig. 1 (*panel A*). Values are expressed as a percentage relative to that observed in the cells transfected with control siRNA and stimulated with VEGF in the absence of COMP-Ang1. Data are shown as means ± S.D. of three independent experiments. *C*, confluent HUVECs transfected with control or KLF2 siRNA were starved in medium 199 containing 1% BSA for 2 h. The cells prestimulated with (+) or without (−) COMP-Ang1 for 1 h were challenged with vehicle (*control*) or 50 ng/ml VEGF (*VEGF*) for 4 h. PKH67 fluorescent dye-labeled U937 cells were adhered to the HUVEC monolayers for 90 min. After fixation, phase contrast and PKH67 fluorescent (*green*) images were recorded with an Olympus IX-81 inverted fluorescence microscope. Shown are representative merged images. *D*, adhesion of U937 cells to HUVECs observed in *C* was quantified as described under "Experimental Procedures." Values are expressed as a percentage relative to that observed in the cells transfected with control siRNA and stimulated with VEGF in the absence of COMP-Ang1. Data are shown as means ± S.D. of four independent experiments. Significant differences between two groups are indicated as ***, $p < 0.001$. *n.s.* indicates no significance between two groups.

anti-inflammatory effects on the vascular endothelium (19, 24, 25). Ang1 also has anti-inflammatory effects and is known to counteract VEGF-induced inflammation (29, 30). Therefore, we hypothesized that Ang1 may inhibit VEGF-induced inflammation by inducing KLF2. To address this question, by depleting KLF2 using siRNA, we examined the effect of Ang1 through KLF2 on VEGF-induced VCAM-1 expression and VEGF-mediated monocyte adhesion to HUVECs. COMP-Ang1 partly inhibited VEGF-induced VCAM-1 expression and VEGF-induced adhesion of U937 cells to HUVECs (Fig. 7 and supplemental Figs. S4 and S5). However, these inhibitory effects of COMP-Ang1 were blunted by depletion of KLF2 (Fig. 7 and supplemental Figs. S4 and S5). These findings suggest that Ang1 competes with VEGF on inflammation through induction of KLF2.

DISCUSSION

Ang1/Tie2 signal is involved in both angiogenesis and vascular quiescence in adult vasculature. Recently, we and another group have shown that endothelial cell-cell contacts specify downstream signaling pathways from Tie2 (10, 11). In the presence of cell-cell contacts, Ang1 induces *trans*-association of Tie2, leading to a preferential activation of the AKT pathway. In addition, we also found that KLF2 is specifically induced by *trans*-associated Tie2. Because KLF2 is a transcription factor involved in vascular quiescence, we hypothesized that KLF2 is responsible for Ang1/Tie2 signal-mediated vascular quiescence. To address this possibility, we tried to delineate the signaling pathways involved in Ang1-induced KLF2 expression. We found that Ang1/Tie2 signal stimulates transcriptional activity of MEF2 through a PI3K/AKT pathway, which in turn induces KLF2 expression.

MEF2 plays important roles not only in muscle development but also in regulation of blood vessels (21–23). MEF2C has been implicated as a regulator of endothelial integrity and permeability (21). Interestingly, MEF2C-deficient mice exhibit a similar defect in vascular development to KLF2-null mice (52). Our present data demonstrated that MEF2 is indispensable for Ang1-induced KLF2 expression. Therefore, defect of vascular development in Ang1-deficient mice might be partly due to the lack of MEF2-dependent KLF2 induction.

Several posttranslational modifications of MEF2 in the regulation of MEF2-mediated transcription has been reported (49). Among them, ERK5 regulates MEF2 transcriptional activity by phosphorylating its transcription activation domain (36, 43, 44). Parmar *et al.* (19) have reported that flow-mediated increase in KLF2 expression occurs via an ERK5/MEF2 pathway. Because ERK5 is essential for maintaining blood vessel integrity and is known to be stimulated by Ang1 (21, 22, 53), we examined whether ERK5 acts downstream of Ang1/Tie2 to induce KLF2 expression. Unexpectedly, Ang1 only stimulated the ERK5 activity in the absence of cell-cell contacts, and under this condition, KLF2 induction by Ang1 did not occur. Furthermore, knockdown of ERK5 did not prevent Ang1-induced KLF2 expression. Therefore, ERK5 appears to be dispensable for Ang1-induced KLF2 expression.

Our data show that Ang1/Tie2 signal utilizes a PI3K/AKT pathway instead of ERK5 to induce MEF2-dependent KLF2 expression. Similarly, it has been reported that a PI3K/AKT/

MEF2 pathway is used for insulin-like growth factor-induced myogenin expression (54). Huddleson *et al.* (42) have also shown that induction of KLF2 by shear stress requires a PI3K/chromatin-remodeling pathway. In contrast to our result, they claimed that AKT is not involved in this pathway, although it is activated by shear stress. We propose the involvement of AKT in Angl-mediated KLF2 induction because 1) AKT inhibitor and knockdown of AKT both inhibit KLF2 mRNA and protein expression by COMP-Angl; 2) AKT-CA induces the MEF2-dependent transcription and stimulates the KLF2 promoter cooperatively with MEF2; and 3) overexpression of AKT-CA induces both mRNA and protein expression of KLF2 in HUVECs. Currently, the reason for this discrepancy remains unclear, but it may be due to the different cell types used for the experiments. We performed the experiments with HUVECs, whereas they used an EOMA cell line. Alternatively, different stimuli such as Angl and shear stress may trigger distinct signaling pathways downstream of PI3K to stimulate KLF2 induction.

At present, a molecular link between AKT and MEF2 is still unknown. Recently, it has been reported that AKT directly phosphorylates transcriptional coactivator p300, leading to the association of MyoD with p300 and p300/CBP-associated factor (PCAF) (55). In addition, it has been also shown that p300 can physically interact with MEF2 as well as MyoD and enhances their transcriptional activity (28). Importantly, shear stress is shown to induce recruitment of p300 and PCAF into the KLF2 promoter (42). Therefore, the Angl/Tie2/PI3K/AKT pathway may induce the association of MEF2 with transcriptional coactivators such as p300 and PCAF, thereby stimulating its transcriptional activity. p300 directly acetylates and stimulates MEF2 activity (51). However, PI3K-mediated activation of MEF2 is not mediated by such direct acetylation mechanism because transcriptional activity of acetylation-defective mutant of MEF2 could be stimulated by constitutive active PI3K (supplemental Fig. S3). Thus, further examination is required for clarifying the molecular link between AKT and MEF2.

KLF2 inhibits VEGF-induced angiogenesis and inflammation, possibly by maintaining vascular quiescence. Similarly, Angl counteracts VEGF-mediated inflammatory responses. Our present data suggest that inhibition of VEGF-mediated inflammatory responses by Angl depends upon KLF2. However, Angl also acts cooperatively with VEGF to induce angiogenesis in a certain situation (5, 7, 9). This opposite effect of Angl on VEGF-mediated responses may depend upon whether KLF2 is induced or not. In the presence of cell-cell contacts, Angl/Tie2 signal is able to induce KLF2 expression and thereby inhibits VEGF-induced inflammation and angiogenesis. However, in the absence of cell-cell contacts, Angl/Tie2 signal accelerates angiogenic signal because KLF2 is not induced in this condition, which accounts for the cooperation of Angl with VEGF. Therefore, KLF2 may be a key downstream factor from *trans*-associated Tie2 to maintain vascular quiescence.

In conclusion, we found that Angl/Tie2 signal stimulates transcriptional activity of MEF2 through a PI3K/AKT pathway to induce KLF2 expression, thereby contributing to vascular quiescence.

Acknowledgments—We are grateful to M. K. Jain and G. B. Atkins (Case Western Reserve University) for the KLF2-Luc reporter plasmid, to Y. Fujio (Osaka University) for the adenovirus encoding AKT-CA, to C. Grozinger for the expression vector for HDAC5 (Harvard University), to K. Matsuo, M. Sone, M. Minamimoto, M. Maeoka, and Y. Matsuura for technical assistance, and to N. Takakura (Osaka University), M. Murakami (Kyoto University), H. Fujita (Osaka City University), and H. Daitoku (University of Tsukuba) for helpful advice.

REFERENCES

1. Dumont, D. J., Gradwohl, G., Fong, G. H., Puri, M. C., Gertsenstein, M., Auerbach, A., and Breitman, M. L. (1994) *Genes Dev.* **8,** 1897–1909
2. Suri, C., Jones, P. F., Patan, S., Bartunkova, S., Maisonpierre, P. C., Davis, S., Sato, T. N., and Yancopoulos, G. D. (1996) *Cell* **87,** 1171–1180
3. Sato, T. N., Tozawa, Y., Deutsch, U., Wolburg-Buchholz, K., Fujiwara, Y., Gendron-Maguire, M., Gridley, T., Wolburg, H., Risau, W., and Qin, Y. (1995) *Nature* **376,** 70–74
4. Wong, A. L., Haroon, Z. A., Werner, S., Dewhirst, M. W., Greenberg, C. S., and Peters, K. G. (1997) *Circ. Res.* **81,** 567–574
5. Peters, K. G., Kontos, C. D., Lin, P. C., Wong, A. L., Rao, P., Huang, L., Dewhirst, M. W., and Sankar, S. (2004) *Recent Prog. Horm. Res.* **59,** 51–71
6. Brindle, N. P., Saharinen, P., and Alitalo, K. (2006) *Circ. Res.* **98,** 1014–1023
7. Asahara, T., Chen, D., Takahashi, T., Fujikawa, K., Kearney, M., Magner, M., Yancopoulos, G. D., and Isner, J. M. (1998) *Circ. Res.* **83,** 233–240
8. Lin, P., Polverini, P., Dewhirst, M., Shan, S., Rao, P. S., and Peters, K. (1997) *J. Clin. Investig.* **100,** 2072–2078
9. Eklund, L., and Olsen, B. R. (2006) *Exp. Cell Res.* **312,** 630–641
10. Fukuhara, S., Sako, K., Minami, T., Noda, K., Kim, H. Z., Kodama, T., Shibuya, M., Takakura, N., Koh, G. Y., and Mochizuki, N. (2008) *Nat. Cell Biol.* **10,** 513–526
11. Saharinen, P., Eklund, L., Miettinen, J., Wirkkala, R., Anisimov, A., Winderlich, M., Nottebaum, A., Vestweber, D., Deutsch, U., Koh, G. Y., Olsen, B. R., and Alitalo, K. (2008) *Nat. Cell Biol.* **10,** 527–537
12. Kuo, C. T., Veselits, M. L., Barton, K. P., Lu, M. M., Clendenin, C., and Leiden, J. M. (1997) *Genes Dev.* **11,** 2996–3006
13. Lee, J. S., Yu, Q., Shin, J. T., Sebzda, E., Bertozzi, C., Chen, M., Mericko, P., Stadtfeld, M., Zhou, D., Cheng, L., Graf, T., MacRae, C. A., Lepore, J. J., Lo, C. W., and Kahn, M. L. (2006) *Dev. Cell* **11,** 845–857
14. Wu, J., Bohanan, C. S., Neumann, J. C., and Lingrel, J. B. (2008) *J. Biol. Chem.* **283,** 3942–3950
15. Atkins, G. B., and Jain, M. K. (2007) *Circ. Res.* **100,** 1686–1695
16. Dekker, R. J., van Soest, S., Fontijn, R. D., Salamanca, S., de Groot, P. G., VanBavel, E., Pannekoek, H., and Horrevoets, A. J. G. (2002) *Blood* **100,** 1689–1698
17. Huddleson, J. P., Srinivasan, S., Ahmad, N., and Lingrel, J. B. (2004) *Biol. Chem.* **385,** 723–729
18. Dekker, R. J., van Thienen, J. V., Rohlena, J., de Jager, S. C., Elderkamp, Y. W., Seppen, J., de Vries, C. J. M., Biessen, E. A. L., van Berkel, T. J. C., Pannekoek, H., and Horrevoets, A. J. G. (2005) *Am. J. Pathol.* **167,** 609–618
19. Parmar, K. M., Larman, H. B., Dai, G., Zhang, Y., Wang, E. T., Moorthy, S. N., Kratz, J. R., Lin, Z., Jain, M. K., Gimbrone, M. A., Jr., and Garcia-Cardena, G. (2006) *J. Clin. Investig.* **116,** 49–58
20. Kumar, A., Lin, Z., SenBanerjee, S., and Jain, M. K. (2005) *Mol. Cell. Biol.* **25,** 5893–5903
21. Hayashi, M., Kim, S. W., Imanaka-Yoshida, K., Yoshida, T., Abel, E. D., Eliceiri, B., Yang, Y., Ulevitch, R. J., and Lee, J. D. (2004) *J. Clin. Investig.* **113,** 1138–1148
22. Olson, E. N. (2004) *J. Clin. Investig.* **113,** 1110–1112
23. Wang, L., Fan, C., Topol, S. E., Topol, E. J., and Wang, Q. (2003) *Science* **302,** 1578–1581
24. SenBanerjee, S., Lin, Z., Atkins, G. B., Greif, D. M., Rao, R. M., Kumar, A., Feinberg, M. W., Chen, Z., Simon, D. I., Luscinskas, F. W., Michel, T. M., Gimbrone, M. A., Jr., Garcia-Cardena, G., and Jain, M. K. (2004) *J. Exp.*

Med. **199,** 1305–1315
25. Lin, Z., Hamik, A., Jain, R., Kumar, A., and Jain, M. K. (2006) *Arterioscler. Thromb. Vasc. Biol.* **26,** 1185–1189
26. Bhattacharya, R., SenBanerjee, S., Lin, Z., Mir, S., Hamik, A., Wang, P., Mukherjee, P., Mukhopadhyay, D., and Jain, M. K. (2005) *J. Biol. Chem.* **280,** 28848–28851
27. Dekker, R. J., Boon, R. A., Rondaij, M. G., Kragt, A., Volger, O. L., Elderkamp, Y. W., Meijers, J. C. M., Voorberg, J., Pannekoek, H., and Horrevoets, A. J. G. (2006) *Blood* **107,** 4354–4363
28. Sartorelli, V., Huang, J., Hamamori, Y., and Kedes, L. (1997) *Mol. Cell. Biol.* **17,** 1010–1026
29. Gamble, J. R., Drew, J., Trezise, L., Underwood, A., Parsons, M., Kasminkas, L., Rudge, J., Yancopoulos, G., and Vadas, M. A. (2000) *Circ. Res.* **87,** 603–607
30. Kim, I., Moon, S. O., Hoon Kim, S., Jin Kim, H., Soon Koh, Y., and Young Koh, G. (2001) *J. Biol. Chem.* **276,** 7614–7620
31. Gavard, J., Patel, V., and Gutkind, J. S. (2008) *Dev. Cell* **14,** 25–36
32. Thurston, G., Suri, C., Smith, K., McClain, J., Sato, T. N., Yancopoulos, G. D., and McDonald, D. M. (1999) *Science* **286,** 2511–2514
33. Thurston, G., Rudge, J. S., Ioffe, E., Zhou, H., Ross, L., Croll, S. D., Glazer, N., Holash, J., McDonald, D. M., and Yancopoulos, G. D. (2000) *Nat. Med.* **6,** 460–463
34. Cho, C. H., Kammerer, R. A., Lee, H. J., Steinmetz, M. O., Ryu, Y. S., Lee, S. H., Yasunaga, K., Kim, K. T., Kim, I., Choi, H. H., Kim, W., Kim, S. H., Park, S. K., Lee, G. M., and Koh, G. Y. (2004) *Proc. Natl. Acad. Sci. U. S. A.* **101,** 5547–5552
35. Sakurai, A., Fukuhara, S., Yamagishi, A., Sako, K., Kamioka, Y., Masuda, M., Nakaoka, Y., and Mochizuki, N. (2006) *Mol. Biol. Cell* **17,** 966–976
36. Marinissen, M. J., Chiariello, M., Pallante, M., and Gutkind, J. S. (1999) *Mol. Cell. Biol.* **19,** 4289–4301
37. Coso, O. A., Montaner, S., Fromm, C., Lacal, J. C., Prywes, R., Teramoto, H., and Gutkind, J. S. (1997) *J. Biol. Chem.* **272,** 20691–20697
38. Murga, C., Fukuhara, S., and Gutkind, J. S. (2000) *J. Biol. Chem.* **275,** 12069–12073
39. Fukuhara, S., Sakurai, A., Sano, H., Yamagishi, A., Somekawa, S., Takakura, N., Saito, Y., Kangawa, K., and Mochizuki, N. (2005) *Mol. Cell. Biol.* **25,** 136–146
40. Fukuhara, S., Marinissen, M. J., Chiariello, M., and Gutkind, J. S. (2000) *J. Biol. Chem.* **275,** 21730–21736
41. Sen-Banerjee, S., Mir, S., Lin, Z., Hamik, A., Atkins, G. B., Das, H., Banerjee, P., Kumar, A., and Jain, M. K. (2005) *Circulation* **112,** 720–726
42. Huddleson, J. P., Ahmad, N., Srinivasan, S., and Lingrel, J. B. (2005) *J. Biol. Chem.* **280,** 23371–23379
43. Kato, Y., Kravchenko, V. V., Tapping, R. I., Han, J., Ulevitch, R. J., and Lee, J. D. (1997) *EMBO J.* **16,** 7054–7066
44. Kato, Y., Zhao, M., Morikawa, A., Sugiyama, T., Chakravortty, D., Koide, N., Yoshida, T., Tapping, R. I., Yang, Y., Yokochi, T., and Lee, J. D. (2000) *J. Biol. Chem.* **275,** 18534–18540
45. Sohn, S. J., Li, D., Lee, L. K., and Winoto, A. (2005) *Mol. Cell. Biol.* **25,** 8553–8566
46. McKinsey, T. A., Zhang, C. L., and Olson, E. N. (2002) *Curr. Opin. Cell Biol.* **14,** 763–772
47. McKinsey, T. A., Zhang, C. L., Lu, J., and Olson, E. N. (2000) *Nature* **408,** 106–111
48. Vega, R. B., Harrison, B. C., Meadows, E., Roberts, C. R., Papst, P. J., Olson, E. N., and McKinsey, T. A. (2004) *Mol. Cell. Biol.* **24,** 8374–8385
49. Potthoff, M. J., and Olson, E. N. (2007) *Development (Camb.)* **134,** 4131–4140
50. Han, J., Jiang, Y., Li, Z., Kravchenko, V. V., and Ulevitch, R. J. (1997) *Nature* **386,** 296–299
51. Ma, K., Chan, J. K. L., Zhu, G., and Wu, Z. (2005) *Mol. Cell. Biol.* **25,** 3575–3582
52. Bi, W., Drake, C. J., and Schwarz, J. J. (1999) *Dev. Biol.* **211,** 255–267
53. Deng, Y., Yang, J., McCarty, M., and Su, B. (2007) *Am. J. Physiol.* **293,** C1404–C1411
54. Xu, Q., and Wu, Z. (2000) *J. Biol. Chem.* **275,** 36750–36757
55. Serra, C., Palacios, D., Mozzetta, C., Forcales, S. V., Morantte, I., Ripani, M., Jones, D. R., Du, K., Jhala, U. S., Simone, C., and Puri, P. L. (2007) *Mol. Cell* **28,** 200–213

THE JOURNAL OF BIOLOGICAL CHEMISTRY VOL. 284, NO. 13, pp. 8548–8556, March 27, 2009

FBP17 Mediates a Common Molecular Step in the Formation of Podosomes and Phagocytic Cups in Macrophages*[S]

Received for publication, July 23, 2008, and in revised form, December 29, 2008 Published, JBC Papers in Press, January 20, 2009, DOI 10.1074/jbc.M805638200

Shigeru Tsuboi[‡1], Hidetoshi Takada[§], Toshiro Hara[§], Naoki Mochizuki[¶], Tomihisa Funyu[‖], Hisao Saitoh[‖], Yuriko Terayama[‖], Kanemitsu Yamaya[‖], Chikara Ohyama[**], Shigeaki Nonoyama[‡‡], and Hans D. Ochs[§§]

From the [‡]Infectious and Inflammatory Disease Center, Burnham Institute for Medical Research, La Jolla, California 92037, the [§]Department of Pediatrics, Graduate School of Medical Sciences, Kyushu University, Fukuoka 812-8582, Japan, the [¶]Department of Structural Analysis, National Cardiovascular Center Research Institute, Osaka 565-8565, Japan, the [‖]Oyokyo Kidney Research Institute, Hirosaki 036-8243, Japan, the [**]Department of Urology, Hirosaki University School of Medicine, Hirosaki 036-8562, Japan, the [‡‡]Department of Pediatrics, National Defense Medical College, Saitama 359-0042, Japan, and the [§§]Department of Pediatrics, Research Center for Immunity and Immunotherapy, Seattle Children's Hospital Research Institute, Seattle, Washington 98101

Macrophages act to protect the body against inflammation and infection by engaging in chemotaxis and phagocytosis. In chemotaxis, macrophages use an actin-based membrane structure, the podosome, to migrate to inflamed tissues. In phagocytosis, macrophages form another type of actin-based membrane structure, the phagocytic cup, to ingest foreign materials such as bacteria. The formation of these membrane structures is severely affected in macrophages from patients with Wiskott-Aldrich syndrome (WAS), an X chromosome-linked immunodeficiency disorder. WAS patients lack WAS protein (WASP), suggesting that WASP is required for the formation of podosomes and phagocytic cups. Here we have demonstrated that formin-binding protein 17 (FBP17) recruits WASP, WASP-interacting protein (WIP), and dynamin-2 to the plasma membrane and that this recruitment is necessary for the formation of podosomes and phagocytic cups. The N-terminal EFC (extended FER-CIP4 homology)/F-BAR (FER-CIP4 homology and Bin-amphiphysin-Rvs) domain of FBP17 was previously shown to have membrane binding and deformation activities. Our results suggest that FBP17 facilitates membrane deformation and actin polymerization to occur simultaneously at the same membrane sites, which mediates a common molecular step in the formation of podosomes and phagocytic cups. These results provide a potential mechanism underlying the recurrent infections in WAS patients.

Podosomes (see Fig. 1*A*) are micron-scale, dynamic, actin-based protrusions observed in motile cells such as macrophages, dendritic cells, osteoclasts, certain transformed fibroblasts, and carcinoma cells (1). Podosomes play an important role in macrophage chemotactic migration, which is critical for recruitment of leukocytes to inflamed tissues. Podosomes are both adhesion structures and the sites of extracellular matrix degradation (2). Adhesion to and degradation of the extracellular matrix are essential processes for the successful migration of macrophages in tissues. Podosomes occur in most macrophages and can be observed by differentiating human primary monocytes into macrophages with macrophage-colony stimulating factor-1 (M-CSF-1)[2] and staining the F-actin using phalloidin (3, 4). Podosomes labeled in this way appear as F-actin-rich dots (see Fig. 1*C*). Podosome formation has recently been directly observed *in vitro* and *in vivo* in leukocyte migration through the endothelium, diapedesis (5).

Phagocytosis of bacterial pathogens is one of the most important primary host defense mechanisms against infections. The phagocytic cup (see Fig. 1*B*) is an actin-based membrane structure formed at the plasma membrane of phagocytes, including macrophages, upon stimulation with foreign materials such as bacteria. The phagocytic cup captures and ingests foreign materials, and its formation is an essential first step in phagocytosis leading to the digestion of foreign materials (6, 7). When macrophages are stimulated by foreign materials, podosomes disappear, and phagocytic cups, which are also rich in F-actin, are formed to ingest the foreign materials (see Fig. 1*D*).

Wiskott-Aldrich syndrome (WAS) is an X chromosome-linked immunodeficiency disorder. Patients with WAS suffer from severe bleeding, eczema, recurrent infection, autoimmune diseases, and an increased risk of lymphoreticular malignancy (8–10). The causative gene underlying WAS encodes Wiskott-Aldrich syndrome protein (WASP) (11). WASP deficiency due to the mutation or deletion causes defects in adhesion, chemotaxis, phagocytosis, and the development of hematopoietic cells in WAS patients (10).

* This work was supported, in whole or in part, by National Institutes of Health Grant R01HD042752 (to S. T.). The costs of publication of this article were defrayed in part by the payment of page charges. This article must therefore be hereby marked "*advertisement*" in accordance with 18 U.S.C. Section 1734 solely to indicate this fact.

[S] The on-line version of this article (available at http://www.jbc.org) contains six supplemental figures.

[1] To whom correspondence should be addressed: Dept. of Biochemistry, Oyokyo Kidney Research Institute, 90 Yamazaki, Kozawa, Hirosaki 036-8243, Japan. Tel.: 81-172-87-1221; Fax: 81-172-87-1228; E-mail: tsuboi@oyokyo.jp.

[2] The abbreviations used are: M-CSF-1, macrophage-colony stimulating factor-1; FBP17, formin-binding protein 17; WAS, Wiskott-Aldrich syndrome; WASP, Wiskott-Aldrich syndrome protein; N-WASP, neuronal WASP; WIP, WASP interacting-protein; EFC domain, extended FER-CIP4 homology domain; F-BAR domain, FER-CIP4 homology and Bin-amphiphysin-Rvs domain; PMA, phorbol 12-myristate 13-acetate; GFP, green fluorescence protein; siRNA, short interfering RNA; FITC, fluorescein isothiocyanate; PDZ-GEF, PDZ-guanine nucleotide exchange factor; HEK293 cells, human embryonic kidney 293 cells; HA, hemagglutinin; SH3, src homology 3 domain; dSH3, SH3 domain deletion; GST, glutathione *S*-transferase; , $PI(4,5)P_2$, phosphatidylinositol 4,5-bisphosphate; siFBP, siRNA for FBP17; siC, scrambled control siRNA.

The formation of podosomes and phagocytic cups is severely affected in macrophages from WAS patients (3, 12, 42), suggesting that WASP is involved in the formation of these structures. However, the detailed molecular mechanisms of their formation remain unknown. WASP is complexed with a cellular WASP-interacting partner, WASP-interacting protein (WIP) (13, 14). Recently, two groups (including us) have demonstrated that WASP and WIP form a complex and that the WASP-WIP complex is required for the formation of podosomes (4, 15) and phagocytic cups (16). Here, we identified formin-binding protein 17 (FBP17) as a protein interacting with the WASP-WIP complex and examined the role of FBP17 in the formation of podosomes and phagocytic cups.

EXPERIMENTAL PROCEDURES

Reagents and Antibodies—Recombinant human macrophage-colony stimulating factor-1 (M-CSF-1) was purchased from R&D Systems (Minneapolis, MN). Phenylmethylsulfonyl fluoride, leupeptin, pepstain A, aprotinin, IGEPAL CA-630, paraformaldehyde, saponin, bovine serum albumin, 3-methyladenine, latex beads (3 μm in diameter), phorbol 12-myristate 13-acetate (PMA), human IgG, glycerol, Triton X-100, anti-FLAG monoclonal antibody (M2), and anti-β-actin antibody were purchased from Sigma-Aldrich. The anti-WASP monoclonal antibody, anti-WIP polyclonal antibody, and anti-Myc monoclonal antibody (9E10) were obtained from Santa Cruz Biotechnology Inc. (Santa Cruz, CA). The anti-dynamin-2 antibody was purchased from BD Biosciences. The rat anti-hemagglutinin (HA) monoclonal antibody (3F10) was purchased from Boehringer Ingelheim (Ridgefield, CT). The Cy2-labeled anti-rat IgG was obtained from Jackson ImmunoResearch Laboratories (West Grove, PA).

Yeast Two-hybrid Screening—We screened a human lymphocyte cDNA library (Origene Technology Inc., Rockville, MD) using a full-length WIP as bait. A cDNA encoding full-length WIP was cloned into pGilda (BD Biosciences Clontech). The EGY48 yeast strain was transformed with pGilda-WIP, the human lymphocyte cDNA library, and pSH18–34, a reporter plasmid for the β-galactosidase assay. Transformants were assayed for Leu prototrophy, and a filter assay was performed for β-galactosidase measurement (17).

Cells and Transfection—THP-1 and human embryonic kidney (HEK) 293 cells were purchased from the American Type Culture Collection (Manassas, VA) and cultured in RPMI1640 and Dulbecco's modified Eagle's high glucose medium (Invitrogen), respectively, both supplemented with 10% fetal bovine serum. For human primary monocyte isolation, 10–30 ml of peripheral blood was drawn from healthy volunteers and WAS patients after informed consent was obtained. Monocytes were prepared from peripheral blood samples (10–30 ml) using a monocyte isolation kit II (Miltenyi Biotech Inc., Auburn, CA). Transfection of THP-1 cells and monocytes was performed with a Nucleofector device using a cell line Nucleofector kit V and a human monocyte Nucleofector kit, respectively, according to the manufacturer's instructions (Amaxa Biosystems, Gaithersburg, MD). Transfection of HEK293 cells was performed using SuperFect transfection reagent (Qiagen, Valencia, CA). THP-1 cells and monocytes were co-transfected with the FBP17 constructs and a GFP-expressing plasmid, pmaxGFP (Amaxa Biosystems Inc.), as a transfection marker. The transfection efficiency measured using pmaxGFP was 40–50% for THP-1 cells and 10–20% for monocytes.

RNA Interference—A short interfering RNA (siRNA) for FBP17 and its scrambled control siRNA was synthesized by Dharmacon (Lafayette, CO). The targeting sequence was 5′-CCCACTTCATATGTCGAAGTCTGTT-3′ (18). THP-1 cells and monocytes were transfected with siRNA using a cell line Nucleofector kit V and a human monocyte Nucleofector kit, respectively, and a Nucleofector device. Cells were co-transfected with an fluorescein isothiocyanate (FITC)-conjugated control siRNA, BLOCK-IT (Invitrogen), as a transfection marker. The transfection efficiency measured using BLOCK-IT was 40–50% for THP-1 cells and 10–20% for monocytes.

Immunoprecipitation—For immunoprecipitation of WASP from THP-1 cells, 2×10^7 cells were lysed in buffer A (50 mM Tris-HCl, pH 7.5, 75 mM NaCl, 1% Triton X-100, 1 mM phenylmethylsulfonyl fluoride, 1 μg/ml leupeptin, 1 μg/ml pepstatin A, 1 μg/ml aprotinin). Lysates were centrifuged at 10,000 $\times g$ at 4 °C for 15 min. The supernatant was incubated with 2 μg/ml anti-WASP monoclonal antibody (Santa Cruz Biotechnology) at 4 °C for 2 h and then incubated with anti-mouse IgG agarose (Sigma). The resin binding the immune complex was washed three times with 0.5 ml of buffer B (50 mM Tris-HCl, pH 7.5, 10% glycerol, 0.1% Triton X-100), and the complex was eluted with 1× Laemmli's SDS-PAGE sample buffer. Eluted proteins were subjected to SDS-PAGE and analyzed by immunoblotting for WASP, WIP, and FBP17.

GST Pull-down Assay—Glutathione *S*-transferase (GST) and a fusion protein of GST and the src homology 3 (SH3) domain of FBP17 (548–609 amino acids) (GST-FSH3) were purified from *Escherichia coli* (XL-1B) extracts using glutathione-Sepharose-4B. HEK293 cells were transfected with the cDNAs of Myc- or FLAG-tagged protein and lysed in buffer A. Lysates from the transfected cells were incubated with the affinity matrices of GST alone or GST-FSH3 at 4 °C for 1 h. After a 1-h incubation, the matrices were washed five times with buffer A, and pull-down samples were analyzed by immunoblotting using anti-Myc or anti-FLAG antibody.

Immunofluorescence Microscopy—THP-1 cells and monocytes grown on coverslips were differentiated into macrophages by incubation with 12.5 ng/ml PMA (Sigma) and 20 ng/ml M-CSF-1 (R&D Systems), respectively, for 72 h. HEK293 cells were transfected with various cDNA constructs and then cultured on coverslips for 48 h. Cells were fixed with 4% (w/v) paraformaldehyde, permeabilized with 0.1% (w/v) saponin, and blocked with 1% (w/v) bovine serum albumin. Cells were stained with primary antibodies and Alexa Fluor 488- or Alexa Fluor 564-labeled secondary antibodies (Invitrogen). Cells were also stained with Alexa Fluor 568-labeled phalloidin (Invitrogen). Cell staining was examined under a fluorescence microscope (Zeiss Axioplan AR) or an MRC 1024 SP laser point scanning confocal microscope (Bio-Rad).

Assays for the Formation of Podosomes and Phagocytic Cups—The formation of podosomes and phagocytic cups was assayed by visualizing these actin-based membrane structures by F-actin staining as described previously (4, 16). Briefly, podosomes

in differentiated THP-1 cells or macrophages were visualized by F-actin staining with Alexa Fluor 568-phalloidin. To form phagocytic cups in differentiated THP-1 cells or macrophages, latex beads (3 μm, Sigma) were opsonized with 0.5 mg/ml human IgG (Sigma), and cells grown on coverslips were incubated with the IgG-opsonized latex beads at 37 °C for 10 min in the presence of 10 mM 3-methyladenine (Sigma) to stabilize the phagocytic cups (16). The phagocytic cups were then also visualized with Alexa Fluor 568-phalloidin. Cells were examined under a fluorescence microscope (Zeiss Axioplan AR).

Assays for Macrophage Migration and Phagocytosis—For the macrophage migration assay, human macrophages (2×10^5 cells) were plated onto chemotaxis membranes with 5-μm pores (Corning, Acton, MA) coated with 0.15% gelatin/phosphate-buffered saline placed within Boyden chamber inserts. M-CSF-1 was used as a chemoattractant and diluted in serum-containing RPMI 1640 medium in lower chambers. After a 4-h incubation, non-migrating cells were removed by gently wiping the upper surface of the filter. The filter was removed from the inserts using a razor blade and mounted onto glass plates, and the number of migrating cells was counted under a fluorescence microscope. For the phagocytosis assay, human macrophages (1×10^6 cells) were seeded on coverslips and incubated with 0.5 ml of RPMI 1640 medium containing IgG-opsonized latex beads (3 μm) at 4 °C for 10 min, allowing the beads to attach to cells. Phagocytosis was initiated by adding 1.5 ml of preheated RPMI 1640 medium, and the cells were incubated with the beads at 37 °C for 30 min. Control plates were incubated at 4 °C to estimate nonspecific binding of latex beads to the cells. After incubation, the cells were vigorously washed with phosphate-buffered saline, and the number of intracellular latex beads was determined by counting beads within cells under a fluorescence microscope. The percentage of phagocytosis was calculated as the total number of cells with at least one bead as a percentage of the total number of cells counted. At least 100 cells were examined.

Cell Fractionation—To prepare the cytoplasmic and membrane fractions, macrophages (1×10^6 cells) were washed with ice-cold phosphate-buffered saline and suspended in 50 mM Tris-HCl buffer, pH 7.5, containing 1 mM EDTA and proteinase inhibitors as described above. The cell suspensions were sonicated four times on ice for 5 s each using a bath-type sonicator followed by ultracentrifugation at 265,000 × *g* at 4 °C for 2 h. The supernatant was used as the cytosolic fraction, and the pellet was resuspended in 50 mM Tris-HCl, pH 7.5, containing 1 mM EDTA and used as the membrane fraction. Anti-Caspase-3 (Santa Cruz Biotechnology) and anti-sodium potassium ATPase antibodies (AbCam, Inc., Cambridge, MA) were used to determine the purity of the cytosolic and membrane fractions, respectively.

Statistics—Statistically significant differences were determined using the Student's *t* test. Differences were considered significant if $p < 0.05$.

RESULTS

FBP17 Binds to the WASP-WIP Complex and Dynamin-2 in Macrophages—To explore the detailed molecular mechanisms of the formation of podosomes and phagocytic cups, we searched for a protein interacting with the WASP-WIP complex. We identified FBP17 as a WIP-binding protein in a yeast two-hybrid screen using the full-length WIP as bait. FBP17 was originally identified as a protein binding to formin, a protein that regulates the actin cytoskeleton (19). FBP17 is a member of the *Schizosaccharomyces pombe* Cdc15 homology (PCH) protein family (20) and contains an N-terminal extended FER-CIP4 homology (EFC) domain (also known as the FER-CIP4 homology and Bin-amphiphysin-Rvs (F-BAR) domain), protein kinase C-related kinase homology region 1 (HR1), and an SH3 domain (Fig. 1*E*). The EFC/F-BAR domain has membrane binding and deformation activities, and FBP17 is involved in endocytosis in transfected COS-7 cells (18, 21, 22).

To confirm that FBP17 directly interacts with WIP or WASP, we performed GST pull-down assays using a fusion protein of GST and the SH3 domain of FBP17 (GST-FBPSH3). Purified GST and the GST-FSH3 fusion protein were subjected to SDS-PAGE (Fig. 1*F*, *lanes 1* and *2*). The HEK293 transfected cells express the Myc- and FLAG-tagged proteins (Fig. 1*F*, *lanes 3–6*). The results from the GST pull-down assays were shown (Fig. 1*F*, *lanes 7–14*). Both WASP and WIP were pulled down by GST-FSH3 (Fig. 1, *lanes 10* and *14*), indicating that the SH3 domain of FBP17 directly interacts with both proteins.

It has previously been shown that FBP17 binds to N-WASP and dynamin in transfected cells (18, 21). We examined whether FBP17 binds to WASP, WIP, and dynamin-2 in macrophages. THP-1 (human monocyte cell line) cells closely resemble monocyte-derived macrophages when differentiated by stimulation with PMA (23) and form podosomes and phagocytic cups that are morphologically and functionally indistinguishable from those in primary macrophages (supplemental Fig. 1) (4, 16, 23). WASP was immunoprecipitated from the lysates of PMA-differentiated THP-1 cells with an anti-WASP monoclonal antibody (Fig. 1*G*, *lanes 2*, *5*, and *8*) followed by immunoblotting using antibodies to FBP17 (21), WASP, and WIP. Both WIP and FBP17 co-immunoprecipitated with WASP (Fig. 1*G*, *lanes 5* and *8*). FBP17 also co-immunoprecipitated with dynamin-2 (Fig. 1*G*, *lanes 14*). These results, taken together with the results in Fig. 1*F*, suggest that FBP17 binds to the WASP-WIP complex and dynamin-2 in macrophages.

We next used immunofluorescence to examine whether FBP17 localizes at podosomes and phagocytic cups because the WASP-WIP complex is an essential component of podosomes (4, 15) and phagocytic cups (16). THP-1 cells transfected with FLAG-tagged FBP17 (FLAG-FBP17) and differentiated by stimulation with PMA were stained with an anti-FLAG monoclonal antibody to visualize FBP17 and with phalloidin to visualize the F-actin in podosomes and phagocytic cups (Fig. 1, *H* and *I*, *left* and *middle panels*). Merged images revealed that both F-actin and FBP17 are present in podosomes and phagocytic cups (Fig. 1, *H* and *I*, *right panels*), indicating that FBP17 localizes at podosomes and phagocytic cups.

Importance of FBP17 in the Formation of Podosomes and Phagocytic Cups—To determine the importance of FBP17 in the formation of podosomes and phagocytic cups, we knocked down FBP17 in THP-1 cells with siRNAs. To confirm that the expression of FBP17 was knocked down in cells, we transfected THP-1 cells with siRNAs, prepared lysates from the total